OPTICA ACTA

Vol. 4. N° 2 June 1957

# An interference photometer for the measurement of amplitude distributions in diffraction patterns

M. De

Technical Optics Section, Imperial College, London. *

Summary. — *An interference photometer is described which measures the distribution of intensity and phase in the image of a point source. It is a simple modification of the* Mach-Zehnder *type of interferometer, and is essentially an analogue computor for the evaluation of diffraction integrals. The photometric advantage of this method has been discussed in relation to the method of direct scanning. This interference method also gives the distribution of phase directly — a measurement which was not previously possible. The accuracy of the method is found to be greater than that to be expected from direct scanning methods. The effect of a finite size of source has also been studied in respect of the visibility of fringes and its influence on the results obtained.*

Sommaire. — *Description d'un photomètre interférométrique permettant de mesurer la distribution d'intensité et de phase dans l'image d'un point lumineux.*

*C'est une modification simple de l'interféromètre du type* Mach-Zehnder. *Calculateur analogique pour l'évaluation des intégrales de diffraction. L'avantage photométrique de la méthode est discuté par rap port à la méthode de l'exploration directe. Cette méthode interférométrique donne aussi directement la distribution de phase, mesure qui n'était pas possible auparavant. La précision ainsi obtenue est supérieure à celle que l'on peut attendre des méthodes d'exploration directe. L'influence d'une dimension de fini de la source est étudiée également en fonction de la visibilité des franges et de son influence sur les résultats.*

Zusammenfassung. — *Es wird ein Interferenzphotometer beschrieben, welches die Intensität und Phasenverteilung im Bilde einer punktförmigen Lichtquelle zu messen gestattet. Es ist eine einfache Abwandlung des* Mach-Zehnder *schen Interferometers und stellt im Wesentlichen einen Analogrechner für die Auswertung der Diffraktionsintegrale dar. Die photometrischen Vorteile dieser Anordnung werden der Methode der direkten Abtastung gegenübergestellt. Diese Interferenzmethode liefert überdies auch noch unmittelbar die Phasenverteilung, deren Messung vorher gar nicht möglich war. Die Genauigkeit des Verfahrens zeigt sich höher als man es nach der direkten Methode erwarten darf. Es wird ausserdem der Einfluss einer endlichen Grösse der Lichtquelle auf die Sichtbarkeit der Streifen und auf die erhaltenen Ergebnisse untersucht.*

I. **Introduction.** — Accurate measurement of the amplitude and phase distributions in the diffraction images of point sources is necessary for the study of the image forming properties of lens systems. Kingslake and Simmons [1], and Van Heel [2] have used methods involving direct scanning of the diffraction patterns. In these experiments, however, because of the large size of source, the finer structures of the diffraction patterns were not obtained. Nienhuis [3], using a smaller source, also employed the same method. The practical difficulties of this kind of experiment are considerable, because a very small pin-hole source must be used to obtain a diffraction partern which has an intensity distribution sufficiently close to that in the image of a true point source. The total light thus available is very small, and the exploration of the diffraction pattern by a pin-hole aperture of a size comparable with the geometrical image of the source limits still further the amount of light that is used in actual measurement. The accuracy of these measurements is thus severely limited.

In addition to the above limitations methods which measure the intensity directly are not capable of measuring the phase distribution in the diffraction pattern. Nienhuis [3] utilised Zernike's method of the coherent background to obtain a qualitative indication of the phase reversal at each zero of the diffraction pattern. Maréchal [4] employed a mechanical integrator for solving the double integrals that express the amplitude distribution in diffraction images of point sources, but this requires the aberration of the optical system to be measured, and expressed in the form of a polynomial, whose terms are then generated by a special cam.

Hopkins [5] has described the principles of an optical analogue computor for the evaluation of these double integrals, capable of measuring accurately both phase and amplitude in the diffraction image of a point source, and using the actual lens system to be studied. A modified Mach-Zehnder interferometer, based on this principle, is described here, together with its use for the measurement of the diffraction images produced by a defocussed but otherwise aberration-free systems.

II. **Principle of the interference photometer.** — The principle of the photometer will now be given. If an approximately plane wave front emerging from any lens, not necessarily free from aberration, is made to interfere with a reference plane wave front, the intensity at the point $(x, y)$ of the resulting interference pattern is given, apart from a constant factor, by

$$\left| 1 + \exp. \left\{ \mathrm{i}\, k\, W\,(x, y) \right\} \right|^2$$

when the two wave fronts are of equal amplitude and proceed along the same axis. $W\,(x, y)$ represents the wave aberration of the lens system and $k = 2\,\pi/\lambda$ is

* Now at Applied physics Dept. University College of Technology, Calcutta, 9, India.

the propagation constant. If the reference wave front is now tilted such that its normals make angles $\beta$ and $\gamma$ with the meridian and sagittal planes respectively, the intensity at the point $(x, y)$ is given, again apart from a constant factor, by the expression

$$\left| \exp. \left\{ -\mathrm{i}(ux + vy) \right\} + \exp. \left\{ \mathrm{i}\, k\, W(x, y) \right\} \right|^2$$

where $u = -\mathrm{k} \sin \beta . h$, $v = -\mathrm{k} \sin \gamma . h$, and $x, y$ are fractional co-ordinates $x = a/h$ and $y = b/h$ respectively, where $(a, b)$ are the unreduced co-ordinates. The total light flux in the interferogram is therefore given by

(1)

$$\iint \left| \exp. \left\{ -\mathrm{i}(ux + vy) \right\} + \exp. \left\{ \mathrm{i}\, k\, W(x,y) \right\} \right|^2 \mathrm{d}x\, \mathrm{d}y$$
$$= 2 \iint \mathrm{d}x\, \mathrm{d}y + 2 \iint \cos \left\{ k\, W(x,y) + (ux + vy) \right\} \mathrm{d}x\, \mathrm{d}y$$

The first term in the above expression is a constant, while the second term has the same form as the integral expressing the real part of the complex amplitude at a point in the diffraction pattern produced by lens systems, the angular co-ordinates of the point being the angles $\beta$ and $\gamma$ as defined above. Thus, by changing the tilt of the reference plane wave front the whole diffraction pattern may be explored, and from measurements of the total light flux in the resulting fringes one may obtain the real part of the complex amplitude in the image plane under consideration. If, now, by introducing an appropriate path difference, the reference plane wave front is shifted in phase by $\pi/2$, the fringe system changes and the total light flux in this new interferogram will be given by an expression similar to (1) above, the cosine being replaced by a sine. In this way, the imaginary part of the complex amplitude is measured. Knowing both the real and imaginary parts of the complex amplitude enables the phase of the disturbance in the diffraction pattern to be obtained.

III. **Photometric efficiency**. — It is desirable to examine the photometric advantages that this method possesses over conventional direct scanning methods. Firstly, the latter methods have to use a very small pin-hole aperture, the diameter of which should not exceed a quarter of that of the Airy disc (Weinstein [6]). If the luminance of the light source is $L$ cd./cm$^2$, $\sigma$ the radius of the pin-hole aperture, and $\alpha$ the angular semi-aperture of the optical system producing the diffraction pattern, the amount of light contained within the cone accepted by the system is $L\, \pi^2\, \sigma^2 \sin^2 \alpha$. This total light flux will be distributed over the entire diffraction pattern. Considering the most favourable case of an aberration free image, with scanning aperture centred on the centre of the Airy disc pattern, the fraction of light within a circle of radius $u_0'$, in the co-ordinates defined above, of the diffraction pattern is given by

(2) $$1 - J_0^2(u_0') - J_1^2(u_0')$$

where $J_0$ and $J_1$ are the Bessel functions of order zero and unity. The total light, therefore, available through the scanning aperture of radius $u_0'$ and placed at the centre of the diffraction pattern is

$$F = L\, \pi^2\, \sigma^2 \sin^2 \alpha \left\{ 1 - J_0^2(u_0') - J_1^2(u_0') \right\}.$$

If the radius $\sigma$ is made equal to a quarter of that of the Airy disc, $\sigma = \frac{1}{4}(0.61\, \lambda/n \sin \alpha)$, where $\lambda$ is the wavelength of light used then and $u_0' = 0.96$ is the value of the radius, giving.

$$F = 0.05\, \lambda^2\, L \text{ lumens.}$$

This gives 1.8 $\mu$ W of energy if a sodium lamp is used, and about 25 $\mu$ W if a high pressure mercury lamp is used with a filter to isolate the green line. The difficulties associated with precise measurements of such low levels of energy are well-known.

In the interference method described here, one half of the total light is used in measuring the real part of the complex amplitude at the central part of the image produced by an unaberrated wave. Thus, even using the same size of pin-hole source, the amount of light available in the interference method is about five times that obtainable with the direct scanning method for the measurement of the intensity at the centre of the Airy disc. At a point in the diffraction pattern having an amplitude equal to 0.10 times that at the centre of the pattern, the second term in the expression (1) is only reduced by a factor of 0.10, whereas the intensity at such a point is reduced by a factor of 0.01. Hence the gain in efficiency of the interference method over the direct scanning method becomes very much larger for points in the outer parts of the diffraction pattern, thus making possible more precise measurements of the weaker outer rings.

The above comparison is based on the assumption that the size of pin-hole source is the same in both cases. In fact, as will be seen later, a much larger size of source can be used in the interference photometer. Even in our present case, where the magnifications of the optical systems in the two paths of the interferometer were unequal, it was possible to use a source having ten times the radius that could be used in direct scanning photometry, thus giving a further factor of 100 in the light flux to be measured. The size of the pin-hole source in the interference photometer is limited by the conditions of visibility of the interference fringes, and this, as is shown later, could be significantly larger than that actually used in the present measurements.

IV. **Instrumentation**. (a) *Tilting of the reference wave front.* — To explore the diffraction pattern from its centre out to the first dark ring in the case of per-

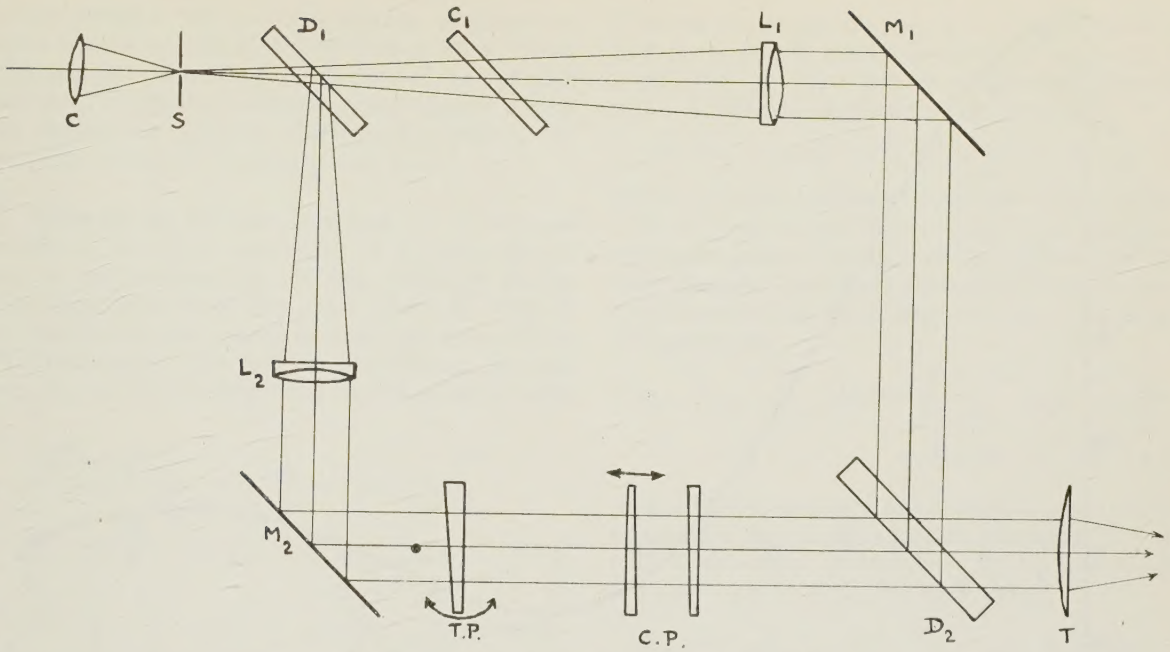


FIG. 1. — Schematic lay out of the interferometer.

fect systems, the tilt of the reference wave front must be varied from zero to an angle equal to $3.83\ \lambda/2\pi h$, where $h$ is the radius of the pupil. With a lens system of 1″ diameter aperture, this tilt will be less than 6 sec. of arc. For a sufficiently detailed exploration of the diffraction pattern, the minimum tilt required is less than a second of arc, while the total range has to be between 20 and 30 secs. in the case of aberrated systems. The smallness of these angles makes conventional methods of tilting a beam of light (for example, reflection by a rotatable mirror) too imprecise.

Accurate tilting of the wave front can be acheived, however, by using a small angle prism (DE, [7]), the change in tilt being obtained by changing the angle of incidence of the wave front on the prism. An angular reduction ratio of 260 : 1 at the normal incidence position was obtained. The prism was rotated by moving one end of a long lever arm on which it was carried. Since the change in deviation produced by the prism does not depend linearly on the change in the angle of incidence, the mechanism had to be calibrated initially.

(b) *Introduction of phase difference.* — To obtain the imaginary part of the complex amplitude, it is necessary to introduce a phase difference between the two interference beams of an amount equal to $\pi/2$. It will be seen later that it is also desirable to be able to vary this path continuously over a number of wave lengths.

The form of the compensator chosen consisted of a pair of identical prisms placed in opposition, the phase difference being obtained by moving one prism longitudinally with respect to the other (HANSEN [8], CANDLER [9]). With prisms of 2° angle, 1 mm displacement of the prism was found to produce about half a wave length of path difference.

With this system, however, a slight lateral shift of the beam also takes place. Such a shift will produce a shear between the two beams, but this was too small to be of any consequence in the present instrument.

(c) *General arrangement.* — A schematic diagram of the interferometer is given in figure 1. It is essentially a MACH-ZEHNDER interferometer, but collimation takes place internally, and separately in each of the two beams. A similar arrangement for collimation has been described by JOHNSON and SCHOLES [10].

In the present case the optical systems in the two arms of the interferometer were different, and the effect of source size on the visibility of interference fringes had consequently to be more closely examined. It was found that, even using two collimating lenses of such differing focal lengths as 300 and 350 mm respectively in the two arms, a source of 50 μ diameter could be used without appreciably impairing the fringe contrast.

An EMI 14-stage multiplier was used for the measurement of the total light flux in the interference pattern, the response of which was directly measured by means of a galvanometer. The light to be measured, being that in an interference pattern whose form changes, it was found necessary to diffuse the light flux before it reached the photocathode of the detector. A pair of crossed transmission gratings of coarse structure was used for the purpose (BAKER [11]). This arrangement has a high transmission factor, being of the order of 95 % in practical cases.

V. **Method of Measurement.** — The adjustment of the apparatus followed closely the methods used in the normal MACH-ZEHNDER interferometer with external collimation. The instrument was first used as an

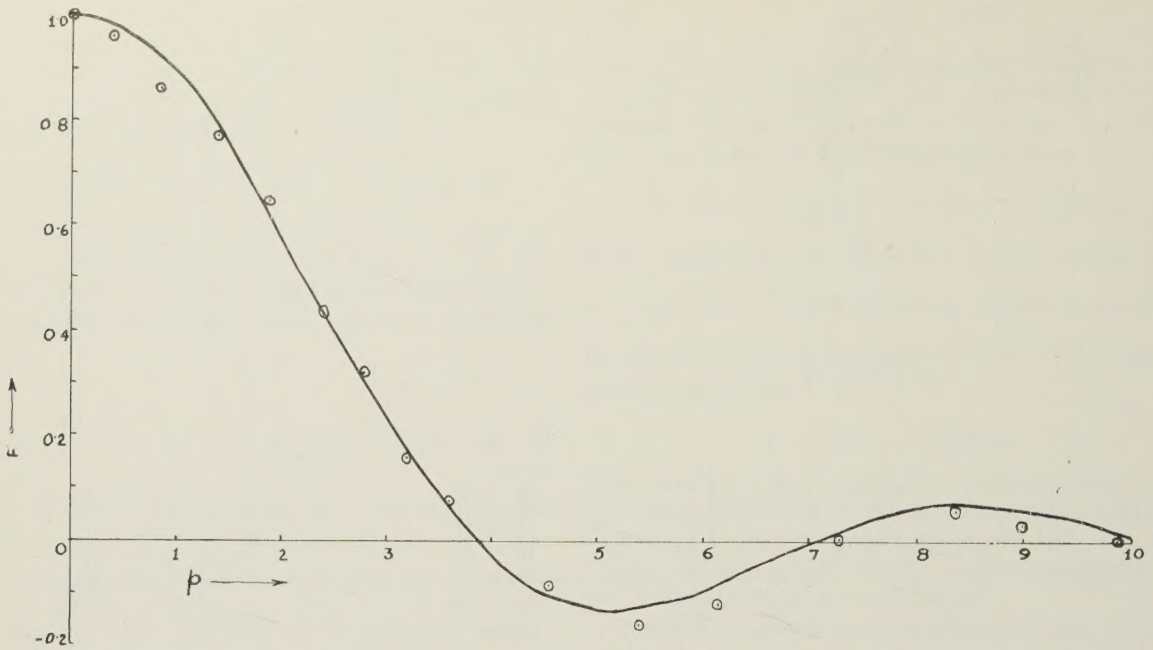


Fig. 2. — Amplitude distribution in gaussian plane for perfect systems.
Negative amplitude indicates phase- shift by $\pi$.
solid curve : theoretical ; encircled dots : experimental points.

$$F = \frac{2\,J_1(p)}{p}\,;\, p = \frac{2\pi}{\lambda}\,n'\sin\alpha'\,\xi'$$

ordinary Mach-Zehnder instrument with external collimation, no lens systems being inserted in the two paths. This arrangement may be utilised to obtain the radial distribution of amplitude and phase in the diffraction pattern that would be produced by a perfect lens system having a circular aperture. It should be noted that even if there were small residual aberrations present in the external collimator the fringe pattern will be unaffected by it. Figure 2 shows the results obtained in this way using sodium vapour lamp as the light source. Negative amplitude shown in the figure indicates phase reversal only.

To study the diffraction pattern in out-of-focus planes by a perfect system, two good quality lens systems were used in the two paths of the interferometer. Precautions were taken to ensure coincidence after reflection of the optical axes of the two beams in the final image space, and accurate location of the pinhole source on the axis, free from coma and astigmatism.

The experiment, however, can be conducted in two different ways. Recalling equation (1), it will be noted that this was derived on the assumption that the optical path lengths traversed by the two beams are equal. If, however, they differ by an amount $e$, and if the intensities of the two interfering beams are $I_1$ and $I_2$, the intensity at any point $(x, y)$ of the fringe plane is given by

$$\begin{aligned} dC &= \left| \sqrt{I_1}\exp.\left\{-\mathbf{i}(ux+\varrho y+ke)\right\} + \right. \\ &\qquad \left. + \sqrt{I_2}\exp.\left\{\mathbf{i}kW(x,y)\right\}\right|^2 \\ &= I_1 + I_2 + 2\sqrt{I_1 I_2}\cos\left\{kW(x,y) + ux + \varrho y + ke\right\}. \end{aligned}$$

The total light flux in the fringe plane is, therefore, given by

$$\begin{aligned} C &= \iint (I_1 + I_2)\,dx\,dy + 2\iint \sqrt{I_1 I_2} \\ &\qquad \cos\left\{kW(x,y) + ux + \varrho y + ke\right\} dx\,dy \\ &= C_1 + C_2 + 2\sqrt{C_1 C_2}\left\{R(u,\varrho)\cos ke - I(u,\varrho)\sin ke\right\} \\ &= (C_1 + C_2)\left[1 + \frac{2\sqrt{C_1 C_2}}{C_1 + C_2}\,A(u,\varrho)\exp.\left\{\mathbf{i}\,\alpha(u,\varrho)\right\}\right] \end{aligned} \tag{3}$$

where

$$\begin{matrix} R \\ I \end{matrix}(u,\varrho) = \iint \begin{matrix} \cos \\ \sin \end{matrix}\left\{kW(x,y) + (ux+\varrho y)\right\} dx\,dy$$

are the real and imaginary parts respectively of the distribution of the complex amplitude. $A(u, \varrho)$ is, therefore, the modulus of the complex amplitude, and $\alpha(u, \varrho)$ is the phase.

It is apparent from (3) that, if $e$ is varied continuously, $C$ will vary sinusoidally. Thus one may set the phase compensator to obtain a maximum response of the photomultiplier for a given tilt of the reference wave, and then reset the phase compensator for each of a set of different angles of tilt to obtain again the maximum response. This response is then equal to a constant plus a quantity proportional to the modulus of the complex amplitude, and the readings of the compensator give the shift in phase. The alternative way is to set the compensator such that the initial phase difference between the two beams is zero or

$2n\pi$, and measure the photomultiplier response for different values of tilt of the reference wave front, this being proportional to the real part of the complex amplitude. The phase compensator may then be adjusted to introduce a $\lambda/4$ path difference to obtain a response proportional to the imaginary part.

VI. **Influence of the size of source.** — It is now desirable to look into the effect of a finite size of source on the results. Let us, first, consider disturbances originating from the axial point, $S_0$, (fig. 3) of an extended source, which traverse the two arms of the interferometer. The part passing through the lens system, $L_1$, under test will reach the fringe plane with

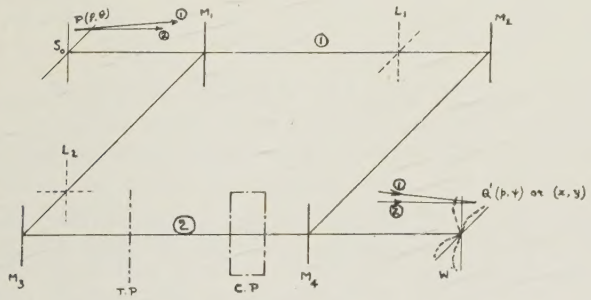


FIG. 3. — Effect of finite source size.

a distribution of phase given by $kW(x, y)$, where $W$ is the aberration of the wave front as a function of the pupil co-ordinates. The other part of the wave front, after passing through the collimator, $L_2$, the tilting mechanism and the phase compensator will reach the same fringe plane and have a distribution of phase over the fringe plane given by $(ux + vy) + ke$, where $ke$ arises from inequality of path lengths, $e$, along the axes of the two paths, and $(u, v)$ are the reduced co-ordinates which measure the tilt of the plane wave front relative to the aberrated one.

The phase difference $\delta_0(x, y)$ between these two wave fronts at $Q'(x, y)$ is given by

$$(4) \quad \delta_0(x, y) = k\,W(x, y) + ux + vy + ke$$

If we now consider the two disturbances which originate from $P(\rho, \theta)$ of the source and reach the same point $Q'(x, y)$, there will be a different phase difference, which will be shown to be given by

$$(5) \quad \delta(x, y) = \delta_0(x, y) + a\,\rho^2 + b\,\rho\cos(\theta - \psi)$$

where $\psi$ is the angular co-ordinate of the point $Q'$.

It has been shown (HOPKINS [5] that the degree of coherence gives a measure of the visibility of interference fringes. The phase coherence factor for the disturbances arriving at $Q'$ from the whole of the source, $\Sigma$ is given by

$$(6) \quad \Gamma_{12} = \frac{1}{\pi\sigma^2}\cdot e^{i\,\delta_0(x,y)} \int_0^{\sigma}\int_0^{2\pi} \exp.\,[i\{a\,\rho^2 + b\,\rho\cos(\theta - \psi)\}]\,\rho\,d\rho\,d\theta$$

where $\sigma$ is the radius of the source, $\Sigma$, over which the integration has to be effected. Denoting, for convenience, the degree of coherence by $V_{12}$ and the phase of $\Gamma_{12}$ by $\delta_0(x, y) + \beta_{12}$, we may write

$$(6\,a) \quad V_{12}\,e^{i\beta_{12}} = \frac{1}{\pi\sigma^2}\int_0^{\sigma}\int_0^{2\pi} \exp.\,[i\{a\,\rho^2 + b\,\rho\cos(\theta - \psi)\}]\,\rho\,d\rho\,d\theta.$$

In the above, $a$ and $b$ are constants involving instrumental parameters only.

The method of evaluation of these constants will consist of finding the two points in the object (source) space which are conjugate to the given point in the fringe plane under consideration for image formation through the two optical systems in the two arms of the interferometer. The phase difference involved in $\delta(\rho, \theta)$ can, then, be determined by considering lengths along appropriate rays in the object space. In this way the geometrical-optical part of the problem may be considerably simplified.

Disturbances from a point $P(\rho, \theta)$ of the source (fig. 4) will radiate outwards equally in all directions. We shall, of course have in mind only those which lie within cones of small apertures. The ray denoted by (1) will travel along one arm of the interferometer and

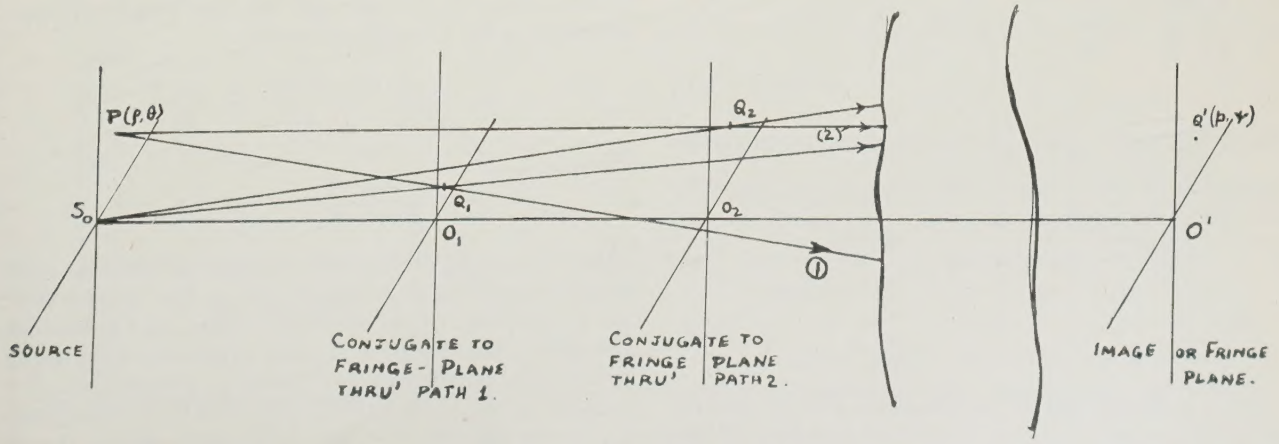


FIG. 4. — Effect of source size.

similarly the ray (2) will traverse along the second arm, both proceeding to the same point Q′ on the fringe plane. These two rays from P will traverse generally unequal path lengths, the optical path difference being given by $[\mathrm{P}\ldots\mathrm{Q}']_1 - [\mathrm{P}\ldots\mathrm{Q}']_2$, where the square brackets denote optical path lengths, and the suffixes denote the different paths followed by the two rays.

Let $Q_1$ and $Q_2$ be the paraxial conjugate points in the object space of Q′ associated with image formation through (1) and (2) respectively. Within the limits of paraxial imagery, optical paths measured along $Q_1$ to Q′ or $Q_2$ to Q′ will be equal. The error in this approximation, for any ray, is, of course, the wave front aberration for that ray. The above path difference from P to Q′ is then given by

$$[\mathrm{P}\ldots\mathrm{Q}']_1 - [\mathrm{P}\ldots\mathrm{Q}']_2 = [\mathrm{PQ}_1 - \mathrm{PQ}_2] + [\mathrm{Q}_1\ldots\mathrm{Q}']_1 - [\mathrm{Q}_1\ldots\mathrm{Q}']_2.$$

To obtain a corresponding expression for the path difference between disturbances from the axial point of the source, which reach the point Q′ on the fringe plane, we consider rays $\mathrm{S}_0\,\mathrm{Q}_1\ldots\mathrm{Q}'$, and $\mathrm{S}_0\,\mathrm{Q}_2\ldots\mathrm{Q}'$ for the two paths respectively. The optical path difference in this case is then

$$[\mathrm{S}_0\mathrm{Q}_1\ldots\mathrm{Q}']_1 - [\mathrm{S}_0\,\mathrm{Q}_2\ldots\mathrm{Q}']_2 = [\mathrm{S}_0\,\mathrm{Q}_1 - \mathrm{S}_0\,\mathrm{Q}_2] + [\mathrm{Q}_1\ldots\mathrm{Q}']_1 - [\mathrm{Q}_2\ldots\mathrm{Q}']_2.$$

We find, finally,

$$\delta - \delta_0 = k\{[\mathrm{PQ}_1 - \mathrm{PQ}_2] - [\mathrm{S}_0\,\mathrm{Q}_1 - \mathrm{S}_0\,\mathrm{Q}_2]\} \tag{7}$$

or

$$\delta = \delta_0 + k\{[\mathrm{PQ}_1 - \mathrm{PQ}_2) - [\mathrm{S}_0\,\mathrm{Q}_1 - \mathrm{S}_0\,\mathrm{Q}_2]\}.$$

If the direction cosines of the rays $\mathrm{S}_0\,\mathrm{Q}_1$ and $\mathrm{S}_0\,\mathrm{Q}_2$ are $L_1$, $M_1$, $N_1$ and $L_2$, $M_2$, $N_2$ respectively and $d_1$ and $d_2$ are the distances of the conjugate planes containing $Q_1$ and $Q_2$ respectively from the source plane, it may be shown that, to a sufficient order of accuracy, the difference term in (7) is equal to

$$k\left\{\frac{1}{2}\left(\frac{N_1}{d_1} - \frac{N_2}{d_2}\right)\rho^2 + \sqrt{[(L_2 - L_1)^2 + (M_2 - M_1)^2]}\;\rho\cos(\theta - \psi)\right\}$$

where $\psi = \tan^{-1}\dfrac{L_2 - L_1}{M_2 - M_1}$, and $(\rho, \theta)$ are the polar coordinates of the point P. On comparison with (5), therefore, we obtain

$$a = \frac{1}{2}\,k\left(\frac{N_1}{d_1} - \frac{N_2}{d_2}\right)$$
$$b = k\sqrt{[L_2 - L_1)^2 + (M_2 - M_1)^2]}. \tag{8}$$

It is a simple matter to obtain $d_1$ and $d_2$ and the direction cosines of the ray concerned, so that it is now possible to effect the integration (6a) in terms of Lommel's U-and V-functions and to evaluate the results numerically to obtain the visibility and phase shift of the fringes across the fringe plane.

We should now look into the effects of the finite size of source on the results that are obtained from the interferometer. Because of the finite size of source of radius $\sigma$, the intensity at the point $(x, y)$ of the fringe plane is given by

$$\mathrm{d}C = 2\,I_1 + 2\,I_1\,V_{12}\cos(\delta_0 + \beta_{12}).$$

Therefore, the total light flux in the pattern is given by

$$C = 2\,C_1 + 2\,C_1\left\{\iint V_{12}\cos(kW + ux + vy)\cos(\beta_{12} + ke)\,\mathrm{d}x\,\mathrm{d}y\right\} - 2\,C_1\left\{\iint V_{12}\sin(kW + ux + vy)\sin(\beta_{12} + ke)\,\mathrm{d}x\,\mathrm{d}y\right\}.$$

Assuming $V_{12}$ to be near enough constant over the fringe plane, an assumption which we shall justify below, we obtain

$$C = 2\,C_1\left[1 + V_{12}\left\{\iint \cos(kW + ux + vy)\cos(\beta_{12} + ke)\,\mathrm{d}x\,\mathrm{d}y - \iint \sin(kW + ux + vy)\sin(\beta_{12} + ke)\,\mathrm{d}x\,\mathrm{d}y\right\}\right].$$

If $\beta_{12}$ is also uniform over the fringe plane, the effect of the finite size of source is only to introduce a scale factor for the modulus of the complex amplitude and a shift of origin for the phase.

The above is, of course, on the assumption that $V_{12}$ and $\beta_{12}$ are constant over the fringe plane, which we shall justify now. From a consideration of the optical circuit followed by the rays in the interferometer sketched in fig. 1, would show that

$$a = \frac{\pi}{\lambda}\left[\frac{(F_2 - F_1)^2}{F_1 F_2^2} + \frac{\epsilon}{F_2^2}\right]$$
$$b = \frac{2\pi}{\lambda}\left(\frac{1}{F_1} - \frac{1}{F_2}\right).\,p \tag{9}$$

where $F_1$ and $F_2$ are the focal lengths of the lens systems in arms 1 and 2 respectively, $p$ the radius vector of the point Q′ on the fringe plane, and $\epsilon$ denotes the equivalent distance of glass thickness, separation between principal planes of the lens systems, etc..

If $F_1 = F_2$, $a = \pi\epsilon/\lambda F_2$, and $b = 0$. In this case, $\beta_{12} = 0$, and $V_{12} = \sin(a\sigma^2)/(a\sigma^2)$, which shows that $V_{12}$ is constant over the fringe plane. This allows

quite a large value of $\sigma$ before the visibility would drop below, say, 0.80.

If, however, $F_1 \neq F_2$, the value of $b$ will not be zero, so that we shall have a finite value of $\beta_{12}$, $V_{12}$ and $\beta_{12}$ both varying across the fringe plane. The maximum value of the exponent of $e^{ia\rho^2}$, which appears in the integrand of (6), will, in general, still be quite small. In the case of our instrument, we had $F_1 = 300$ mm and $F_2 = 350$ mm. Assuming $\lambda = 0.0005$ mm, the exponent attains a maximum value of $\pi\sigma^2/7.35$, so that even with $\sigma = 0.15$ mm the maximum value of the exponent will not exceed 0.01. The presence of $\beta_{12}$ may, therefore, be safely ignored.

If this factor is ignored, the value of $V_{12}$ is then given by

$$\frac{2}{\sigma^2}\int_0^{\sigma} J_0(b\rho)\,\rho\,d\rho = 2\,J_1(b\sigma)/(b\sigma).$$

Since $b$ is a function of $p$, the radial distance of the point on the fringe plane from the axis, $V_{12}$ will vary across the fringe plane. This means in effect that the factor $V_{12}$ should be included under the integral in the expression (3) for the total light flux in the interference pattern. The significance, then, is that the total light flux would give a measure of the distribution of amplitude in the diffraction pattern produced by waves having radial inhomogeneity of amplitude. Hopkins [5] showed that in the case where the amplitude decreases from unity at the centre to 0.5 at the margin, the variation being a linear function of the square of the aperture, the results show insignificant departures from the ideal curve. Thus, we may safely tolerate a value of $b$ which would result in $V_{12}$ dropping to, say, 0.7 at the margin of the fringe area, without introducing any appreciable error in our results. In our present case, a source of radius equal to 0.025 mm could be used, which results in a value of $V_{12} = 0.70$ at the margin.

VII. **Experimental results.** — Figure 5 gives the results for the axial distribution of amplitude and phase, the inset showing the sinusoidal variation of

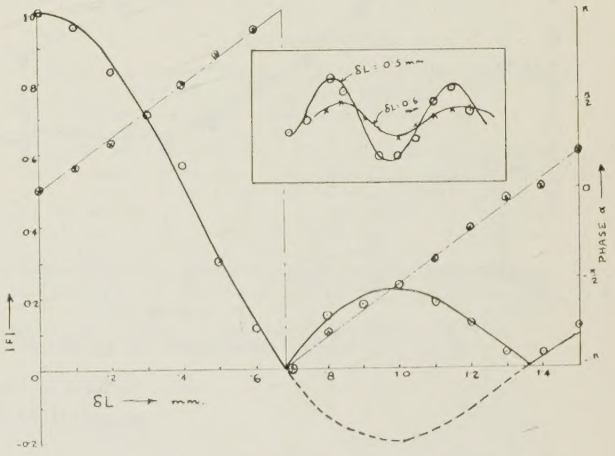


Fig. 5. — Central amplitude (modulus) and phase along the axis of a good F/12. 1″ aperture lens.
*a*) — theoretical amplitude curve ;
*b*) —·— geometrical phase curve.
Inset shows sinusoidal variation of light flux with path-difference $\delta$ for two typical cases.

light flux with change in path difference for two typical cases. Figure 6 gives the radial distribution of

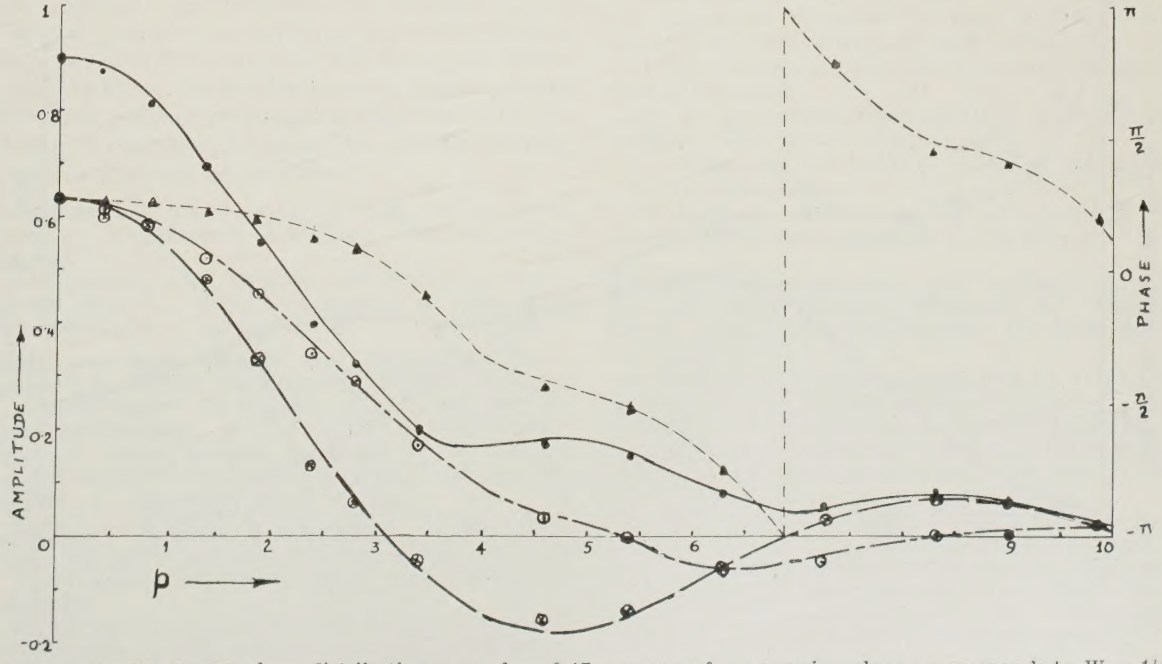


Fig. 6. — Amplitude and phase distribution on a plane 0.17 mm away from gaussian plane ; corresponds to $W = 1/4\,\lambda$.
—— modulus of amplitude $|F|$ ;
— — real part of complex amplitude : $F \cos\alpha$ ;
—·— imaginary part of complex amplitude : $F \sin\alpha$ ;
····· phase $\alpha$.

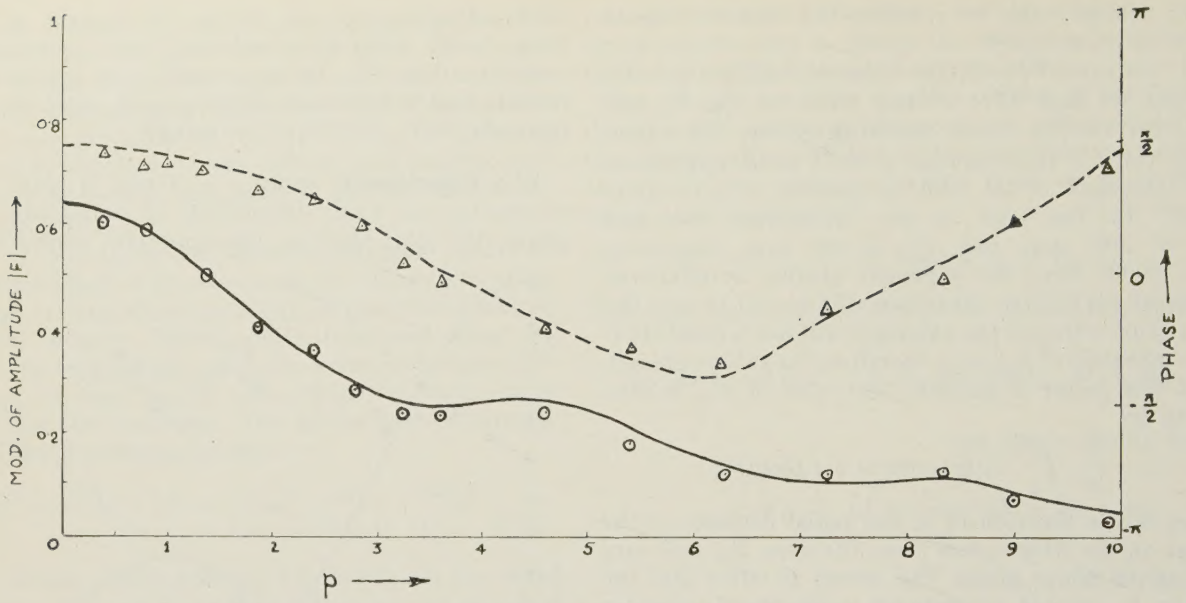


Fig. 7. — Radial distribution of amplitude and phase on an image plane for which $W = 1/2\,\lambda$.
—— modulus of amplitude $\left[ p = \frac{2\pi}{\lambda} n' \sin \alpha' \xi' \right]$;
..... phase.

complex amplitude over an out-of-focus plane (corresponding to a wave front aberration of $\frac{1}{4}\,\lambda$ at the margin), which had been determined utilising both methods suggested before. Two more cases were studied, namely the cases of out-of-focus planes corresponding to wave aberrations of $\frac{1}{2}\,\lambda$, and $\lambda$ at the margin. The results are shown in figures 7 and 8. In drawing the curves and plotting the points for these out-of-focus cases, the results were suitably normalised to make the central amplitude and phase equal

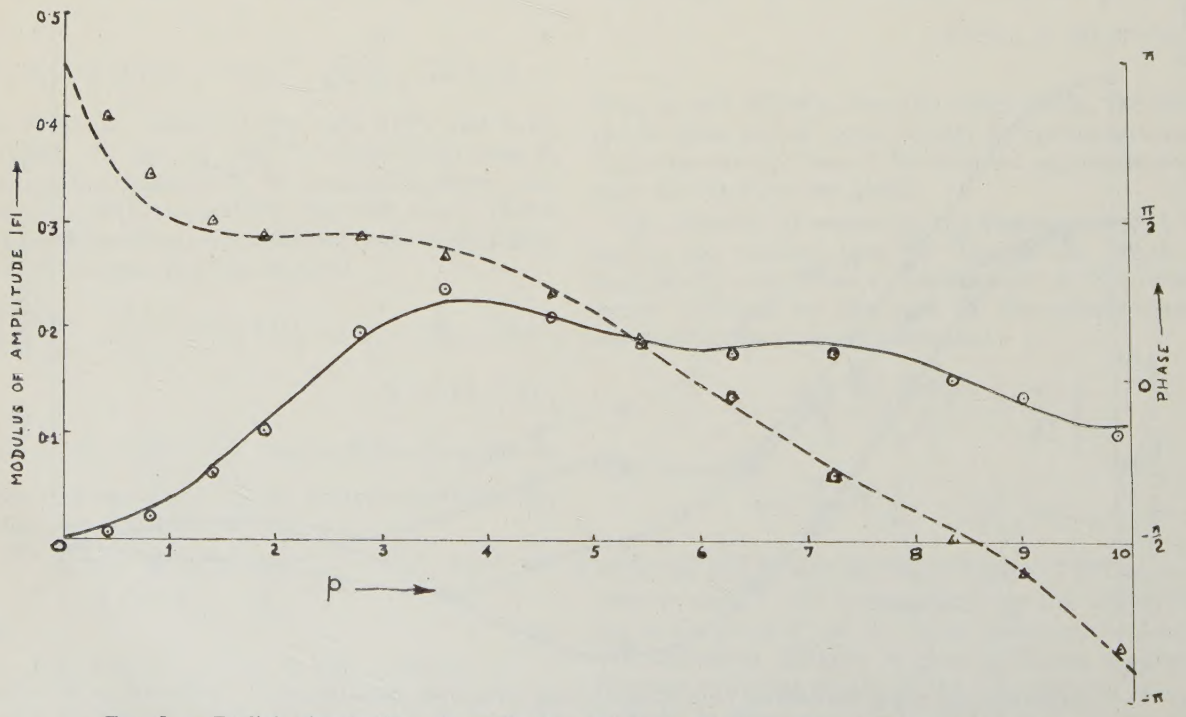


Fig. 8. — Radial distribution of amplitude and phase on an image plane for which $W = 1\,\lambda$.
—— modulus of amplitude;
..... phase.

to the normalised values obtained on the axial distribution curve for the focal plane being measured.

It will be noticed that the phase variation along the axis is found to be linear and given by $\frac{1}{2}kW$, which is, in fact, the geometrical phase term only. Phase distribution curves are also obtained and shown in the figures. The results thus obtained show good aggreement with the theoretical values calculated using the classical formulae of LOMMEL. The reason why the present measurements fail to show the anomalous propagation of phase through the focus appears to be that we use fundamentally the interference effects of two waves, each of which show anomalous propagation of phase. The phase measured by the interferometer is, therefore, the geometrical phase relations along the axis, the two phase anomalies cancelling each other.

VIII. **Acknowledgements.** — The author is indebted to Dr H. H. HOPKINS for suggesting the problem and also for his constant guidance and stimulating criticism throughout the work. Thanks are also due to the Government of India and the University of Calcutta for the provision of a maintenance grant during the period the work was done. The latter part of this work was carried out under a contract from the Ministry of Supply.

*Manuscrit reçu le 24 septembre 1956.*

REFERENCES

1. KINGSLAKE and SIMMONS, *J. O. S. A.*, **23**, 1933, 283.
2. A. C. S. VAN HEEL, *Physica*, **2**, 1935, 62.
3. K. NIENHUIS, Thesis, Groningen Univ., 1948.
4. A. MARÉCHAL, Thesis, Paris Univ., 1948.
5. *a)* H. H. HOPKINS, *Opt. Acta*, **2**, 1955, 23. *b)* H. H. HOPKINS, *Proc. Roy. Soc.*, **208**, 1951, 263 ; *c)* H. H. HOPKINS, *Proc. Phys. Soc.*, B vol. 62 1949.
6. W. WEINSTEIN, *J. O. S. A.*, **45**, 1955.
7. M. DE, *J. Sci. Instr.*, **32**, 1955, 141.
8. G. HANSEN, *Zeit. f. Instr.*, **50**, 1930, 460.
9. C. CANDLER, *Modern Interferometers*, 1951, Hilger.
10. JOHNSON Y SCHOLES, *Australian Jour. of Sci. Res.*, 1 A, 465, 1948.
11. L. R. BAKER, *J. Sci. Instr.*, **32**, 1955, 418.

## BIBLIOGRAPHIE

**Handbuch der Physik.** Vol. XXIV (Optique) Lange, Maxwell, Springer.

Il est probablement superflu de présenter la nouvelle édition du Handbuch der Physik dont on voit fréquemment paraître de nouveaux volumes. Il s'agit maintenant d'un traité international de physique où les articles sont rédigés en l'une des trois langues allemande, anglaise ou française. Le volume XXIV (656 pages) consacré à l'Optique vient de paraître récemment ; on y trouvera, sous une forme très accessible aux étudiants, les développements fondamentaux sur l'optique, poussés jusqu'aux applications actuelles telles que le contraste de phase, les couches minces, etc., etc. Le contenu est le suivant :

*Determination of the Velocity of Light* by DR ERIK BERGSTRAND, Observatory Stockholm (Sweden) (with 31 figures).

*A.* Introduction, *B.* Méthodes of determination in vacuo and in air, *C.* Velocity in matter, *D.* Some relativistic experiments. References.

*Optique géométrique générale*, par ANDRÉ MARÉCHAL, Professeur à la Faculté des Sciences, Institut d'Optique, Paris (France) (avec 208 figures). *A.* Lois générales de l'optique géométrique, *B.* Recherche du stigmatisme rigoureux, *C.* Approximation de Gauss, *D.* Le champ, *E.* Les aberrations, *F.* Contraste des images ; influence des aberrations, *G.* Conclusion. Bibliographie.

*Interférences, diffraction et polarisation*, par MAURICE FRANÇON, Maître de conférences à la Sorbonne, Professeur à l'Institut d'Optique, Paris (France) (avec 427 figures).

*A.* Interférences : I. Introduction sur les vibrations, II. Interférences à deux ondes, III. Interférences à ondes multiples, IV. Application des interférences.

*B.* Diffraction : I. Diffraction de Fraunhoffer ou diffraction à l'infini, II. Diffraction de Fresnel ou diffraction à distance finie.

*C.* Polarisation : I. Polarisation par réflexion, II. Polarisation par double réfraction, III. Etude de la lumière transmise par une lame cristalline éclairée en faisceau parallèle, IV. Interférences en lumière polarisée.

Bibliographie sommaire.

*Optik dünner Schichten*, von DR HANS WOLTER, Professor für Angewandte Physik an der Universität Marburg (Deutschland) (mit 41 Figuren).

I. Allgemeine Übersichtüber die Optik dünner Schichten und die Stoffauswahl in dem vorliegenden Artikel.

II. Die Grundlagen und die Grundaufgabe der Optik dünner Schichten .

III. Reflexionsfreie Schichtsysteme und linearpolarisierend reflektierende Schichtsystem.

IV. Steigerung der Reflexion durch dünne Schichten.

V. Interferenzfilter.

VI. Methoden zur Messung der optischen Konstanten und der Dicke dünner Schichten. Literatur.

*Schlieren Phasenkontrast und Lichtschnittverfahren*, von DR HANS WOLTER, Professor für Angewandte Physik an der Universität Marburg (Deutschland) (mit 54 Figuren).

*A.* Übersicht, *B.* Schlierenverfahren : I. Geometrisch-optische Betrachtung der Schlierenverfahren, II. Zum quantitativen Zusammenhang zwischen Lichtablenkungen und ihren physikalische Ursachen. III. Die Beugungsunschärfe bei Schlierenverfahren und ihre Herabsetzung durch Minimumstrahlkennzeichnung.

*C.* Die Beugung am Objekt bei abbildenden Schlierenverfahren und das Phasenkontrastverfahren nach Zernike : I. Die Beugung am Objek und ihre Wirkung auf die Schlieren und Phasenkontrasbilder einfacher Objektformen, II. Ausführungsformen der Phasenkontrast geräte ; variabler und farbiger Phasenkontrast.

*D.* Das Lichtschnittverfahren.

*E.* Vergleich der Schlieren-und Phasenkontrastverfahren mit den abbildenden Interferenzverfahren.

Literatur.

# Considérations sur la génération des surfaces toriques en optique de lunetterie

A. DEMUYNCK
Ingénieur conseil à la Société OPTIBEL

SOMMAIRE. — I. *Les surfaces toriques du 4e degré utilisées en lunetterie peuvent, du point de vue de leur réalisation pratique, se diviser en 2 classes : le type « Roue » et le type « Fuseau ».*

*Des considérations géométriques montrent que le type « Roue », le plus généralement utilisé, donne lieu à d'inévitables déformations sur une large bande centrale du verre tandis que le type « Fuseau » permet une réalisation précise et de qualité parfaite.*

II. *Dans un deuxième paragraphe sont développées des considérations géométriques relatives à une méthode universellement pratiquée dans les ateliers de prescription, pour la génération individuelle de surfaces toriques convexes ou concaves, au moyen d'un outil circulaire diamanté. Il y est démontré que la section méridienne du tore engendre la forme d'un ménisque à bord arrondi. Les constructeurs indiquent les réglages correspondant à la partie concave du ménisque. Il est démontré que cette surface concave présente 2 points d'inflexion très accusés, produisant dans les surfaces taillées des déformations importantes tandis que l'arc convexe de la section méridienne est très régulier sur toute sa longueur et ses écarts du cercle sont nettement inférieurs à ceux de l'arc concave.*

*L'utilisation de l'arc convexe exige toutefois un plus profond dégagement de la fraise diamantée.*

ZUSAMMENFASSUNG. — *Die torischen Flächen vierten Grades, die in der Brillenoptik verwendet werden, lassen sich im Hinblick auf ihre praktische Herstellung in zwei Klassen einteilen : die « Radform » und die « Spindelform ». Eine geometrische Betrachtung ergibt, dass die am meisten benutzte Radform notwendigerweise auf einem breiten mittleren Streifen des Glases Abweichungen ergibt, während die Spindelform eine genaue Herstellung mit hoher Flächengüte ermöglicht.*

*Der zweite Abschnitt enthält die geometrische Theorie einer in den Brillenwerkstätten allgemein üblichen Art der individuellen Herstellung torischer Konvex-und Konkavflächen mittels eines runden Diamantwerkzeuges. Der Meridianschnitt des erzeugten Torus hat die Form eines Meniskus mit abgerundetem Rand. Die Konstrukteure geben gewöhnlich nur die Einstellungen für den konkaven Teil des Meniskus. Diese konkave Fläche hat aber zwei sehr hervortretende Wendepunkte, die auf der so hergestellten Fläche ernsthafte Abweichungen bewirken, während der konvexe Bogen des Meridianschnittes in seiner ganzen Ausdehnung sehr regelmässig verläuft und Abweichungen merklich kleiner bleiben als im Falle des Konkavbogens. Die Verwendung des konvexen Teiles erfordert aber eine tiefere Innenkammer des Diamantfräsers.*

SUMMARY. — I. *Toric surfaces of the 4th degree used in spectacles can, from the point of view of production, be divided into two forms, « wheel » and « barrel ». Geometrical considerations show that the « wheel » type, which is the more commonly used, can only be produced with deformations over a large central aera, whereas the « barrel » form can be accurately made.*

II. *In the second part geometric considerations are discussed for a generally applicable method of producing individual toric surfaces, either convex or concave by a circular diamond tool. It is shown that the meridian section of the torus produces the form of a meniscus with a rounded edge. Procedures are given for the concave part of the meniscus. It is shown that this concave surface has two sharp points of inflection producing serious deformations in surfaces produced, while the convex part of the meridian section is very regular over all its length and departs little from a circular form.*

*The use of the convex arc always requires a greater clearance of the diamond lap.*

I. **Travail en série.** Les surfaces toriques utilisées en lunetterie sont des surfaces de révolution, engendrées par la rotation d'un cercle autour d'un axe situé dans son plan.

Si r est le rayon du cercle générateur et a la distance du centre de ce cercle à l'axe de révolution, l'équation du tore engendré sera :

$$[x^2 + y^2 + z^2 + (a^2 - r^2)]^2 - 4a^2 (x^2 + y^2) = 0$$

Du point de vue de la géométrie analytique, il semble indifférent de classer ces surfaces en deux familles distinctes, suivant que $a > r$ ou $a < r$. Il n'en est pas de même du point de vue de leur réalisation pratique, du fait de certaines propriétés géométriques particulières aux deux groupes distincts.

Considérons d'abord le cas $a > r$ ; ceci revient à dire que l'axe de révolution est extérieur au cercle (fig. 1). La surface torique engendrée présente l'aspect d'une chambre à air gonflée. Nous la désignerons par la dénomination : type « ROUE ».

Découpons dans le tore une calotte circulaire, disposée symétriquement de part et d'autre du grand

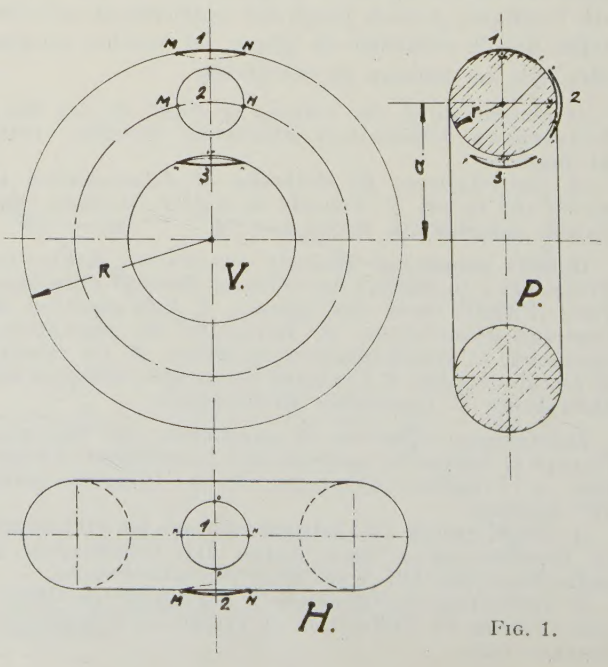


FIG. 1.

cercle parallèle extérieur. Il est évident que l'on peut déplacer cette calotte sur le pourtour le long du grand cercle en conservant la coïncidence parfaite avec le tore. Il n'en sera plus de même si nous déplaçons la calotte dans une direction transversale, par exemple le long d'un petit cercle méridien. Il y a disjonction des surfaces, et la calotte s'appuie sur le tore en 2 points diamétraux M et N. La flèche d'écartement des 2 surfaces s'accentue avec l'élongation transversale, pour être maxima à 180°.

Cette simple constatation géométrique implique une importante conclusion dans le domaine du surfaçage de ces surfaces. Qui dit surfaçage, dit rodages successifs au moyen d'abrasifs de plus en plus fins sur des outils complémentaires aussi parfaits que possible.

La théorie et l'expérience s'accordent pour conclure qu'un surfaçage parfait ne s'obtient que par le croisement continu des directions de frottement en tout point. Il est donc interdit de donner au verre une simple translation le long du grand cercle parallèle dans le but de maintenir la coïncidence parfaite des 2 surfaces ; le résultat serait une surface striée et défectueuse. Il faut combiner ce mouvement avec un déplacement transversal, mais ce dernier mouvement provoque la disjonction des 2 surfaces, et l'appui de la calotte aux seuls points diamétraux M et N. Toute la pression étant concentrée en ces deux points, il se produira en ces points, sous une pression unitaire énorme, une usure très rapide et d'autant plus profonde que l'élongation transversale sera plus grande.

Si la calotte est un verre concave, la surface présentera en M et N des fausses zones en profondeur qui s'étendent rapidement jusqu'au centre (fig. 2). Si la calotte au contraire est l'outil complémentaire concave devant roder des surfaces convexes disposées sur une roue (fig. 3), les points de contact M et N des outils vont entamer en profondeur tous les verres de la roue, sur une bande dont la largeur est fonction de l'élongation transversale, et y inscrire des spirales qu'il sera pratiquement impossible d'effacer ; il en résulte une bande trouble, qui est d'autant plus grave qu'elle couvre le sommet du verre qui ne tolère aucun défaut. Au fur et à mesure que progresse sur l'outil l'usure anormale autour de M et N, la zone régulière de rodage au centre se rétrécit, l'outil n'a plus une assise suffisante et toute précision de surfaçage devient aléatoire.

Examinons à présent la surface torique du second groupe, répondant à la condition $a < r$ (fig. 4). L'axe de révolution est AB. Nous négligeons la surface torique externe, non représentée, engendrée par le grand arc de cercle, pour nous en tenir à la surface torique interne en forme de fuseau.

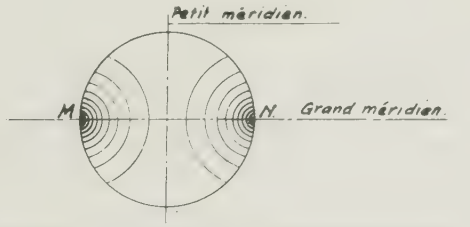


Fig. 2.

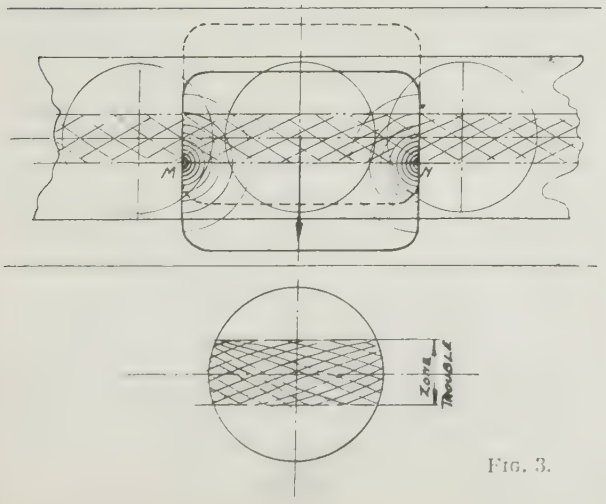


Fig. 3.

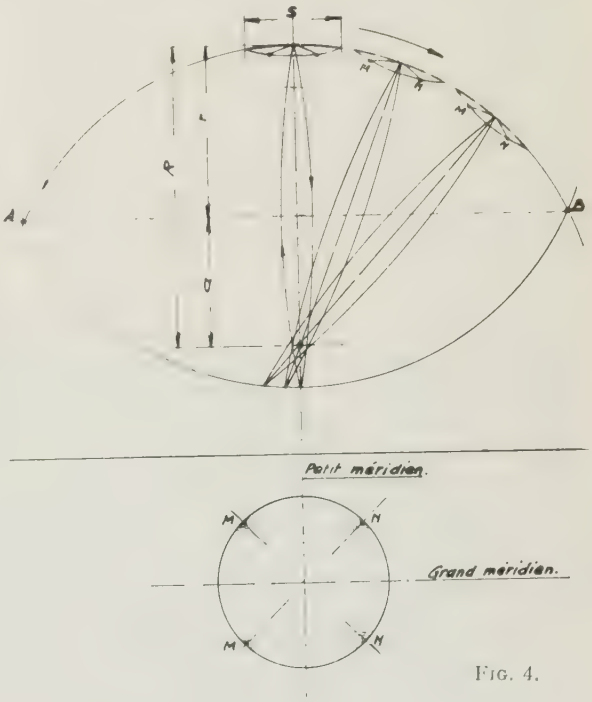


Fig. 4.

Si nous découpons de même une calotte circulaire autour du sommet S, nous constatons immédiatement que nous pouvons la déplacer le long de l'équateur S, sans que la calotte cesse d'être en coïncidence parfaite avec le tore. Un déplacement le long du grand méridien A S B entraîne une légère variation dans la courbure de la section principale perpendiculaire au méridien AB. La section qui au centre S est le petit cercle équateur, devient pour une position excentrée, une légère ellipse. Il en résulte une très minime disjonction aux bords de la calotte, en N pour un déplacement vers la droite, en M pour un déplacement vers la

gauche. En opposition avec le cas précédent, la partie centrale des surfaces reste en contact parfait en toute position, aucun point ou bord tranchant ne pénètre dans la surface complémentaire, et s'il y a une légère disjonction aux extrémités des méridiens bissecteurs de la calotte, la flèche en est si minime, pour des déplacements relativement importants, qu'elle ne dépasse guère l'amplitude des flexions élastiques du verre et ne se traduit en somme que par une variation des pressions de frottement en ces points. La précision et la perfection du surfaçage dans le type « fuseau » sont incomparablement meilleures que dans le type « roue » et si le nombre de verres que l'on peut surfacer sur un outil est plus petit que dans le premier cas, par contre la possibilité d'utiliser des rodoirs et polissoirs de plus amples dimensions, de donner des déplacements transversaux plus grands, l'absence de fausses zones d'usure et de zones troubles, compenseront à tel point ce désavantage, qu'un rendement quantitatif équivalent peut être atteint avec la certitude d'obtenir des surfaces exactes et parfaites.

Devant les considérations géométriques aussi évidentes, dont les conclusions sont parfaitement confirmées par les essais, on est en droit de s'étonner que la méthode « type roue » soit encore si universellement en usage ; il faut sans nul doute incriminer l'espoir d'ailleurs très illusoire d'un rendement quantitatif plus élevé.

II. **Travail d'une surface torique isolée. Surfaçage de prescription.** Il existe sur le marché un type de machine permettant avec un seul outil de coupe (fraise circulaire diamantée) de tailler dans un verre une surface torique quelconque, entre des limites de courbure si étendues qu'elles couvrent pratiquement tout le domaine d'utilisation en lunetterie. L'analyse des principes géométriques mis en œuvre dans cette méthode suggère quelques observations vraisemblablement peu connues puisque les constructeurs de ces machines indiquent universellement les procédés de réglages les moins favorables.

Cette curieuse machine est une ingénieuse transformation d'un procédé vraisemblablement déjà connu de longue date, et qui consiste à tailler un cylindre droit de très faible puissance dioptrique au moyen d'un outil circulaire de diamètre relativement petit (fig. 5).

Une fraise à lames rapportées, dont les pointes tranchantes forment un cercle, est disposé de façon à ce que son axe de rotation fasse avec la verticale un angle $\alpha$. Un déplacement horizontal de cette fraise lui fait décrire dans l'espace un cylindre droit, dont la section droite est une ellipse d'autant plus aplatie que l'angle $\alpha$ est plus voisin de zéro. Cette ellipse est rabattue à gauche dans la figure. Le grand axe ($2\,a$) est du diamètre de la fraise, tandis que le petit $2\,b$ vaut $D$ sin. $\alpha$. Les rayons de courbure en $B_1$ ou $B_2$ valent $\frac{a^2}{b}$, c'est-à-dire $\frac{D}{2 \text{ sin. } \alpha}$. La section obtenue sans doute n'est pas un cercle mais un arc d'ellipse ;

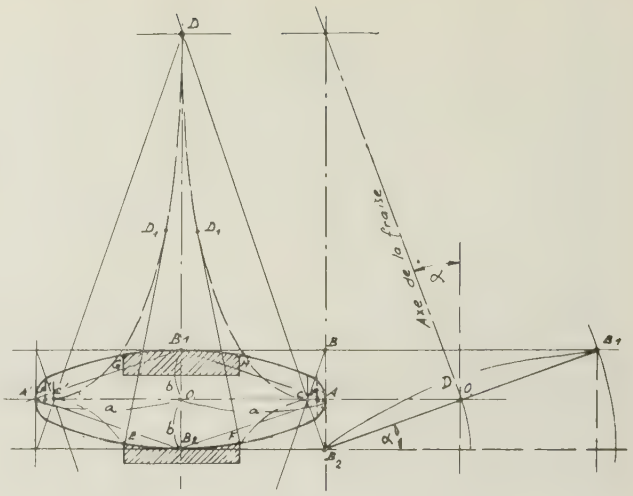


Fig. 5.

toutefois, avec un diamètre suffisant de fraise on obtient un arc d'ellipse suffisamment approché de l'arc de cercle demandé pour les besoins de la lunetterie.

Il est tout indiqué de transformer la translation rectiligne de l'outil en une rotation autour d'un axe perpendiculaire à l'axe du cylindre et à l'axe de la fraise, pour obtenir une surface torique. En effet, les génératrices rectilignes du cylindre deviennent des cercles parallèles dans la révolution du cercle incliné de l'angle $\alpha$ autour du nouvel axe. Dans le cas du cylindre droit, la courbe méridienne taillée dans l'outil est la section elliptique droite du cylindre, donc la projection orthogonale du cercle générateur. Du moment que la surface générée est obtenue par révolution autour d'un axe, la courbe méridienne du tore engendré n'est plus une projection orthogonale du cercle incliné comme ci-dessus, mais doit être obtenue par rabattement autour de l'axe de révolution. La forme de la section méridienne sera donc profondément modifiée, au point qu'un examen géométrique s'impose.

En référence à la fig. 6, si OA est l'axe de la machine, AB la projection horizontale, d'un cercle de centre C

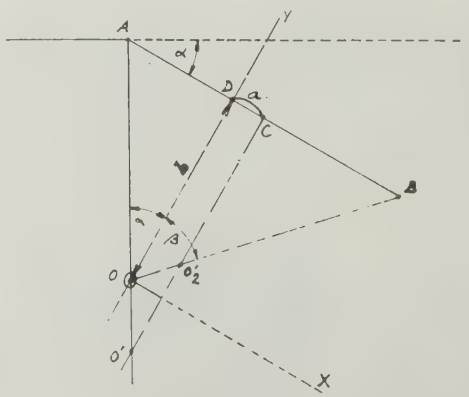


Fig. 6.

situé dans un plan vertical formant avec l'axe l'angle $\alpha$, O le point de percée dans le plan de la figure de l'axe de révolution, pour un cercle de diamètre constant, les seuls paramètres variables du problème seront la distance OA et l'angle $\alpha$ ; ce sont en effet les 2 éléments de réglage de ce type de machine.

Dans un autre type de machine on choisit comme axe de référence la perpendiculaire OD sur le plan du cercle, les paramètres variables sont dès lors la distance OD $= b$ et l'excentration a ; ces deux variables sont équivalentes aux précédentes auxquelles elles sont d'ailleurs liées par des relations simples,

$$\mathrm{OD} = \mathrm{OA} \cos \alpha = \frac{r - a}{\mathrm{tg}\ \alpha}$$

Pour établir l'équation du tore engendré par la révolution du cercle AB autour de l'axe O, considérons un système d'axes rectangulaires avec origine en O, OD étant l'axe des y, l'axe de révolution étant l'axe des z et l'axe des x parallèle au plan du cercle. Les méthodes classiques pour le calcul des surfaces de révolution, donnent facilement l'équation du tore :

$$(x^2 + y^2 + z^2 - (r^2 + b^2 - a^2)\,]^2 - 4\,a^2\,(x^2 + y^2 - b^2) = 0$$

Partant de l'équation de la surface on obtient immédiatement l'équation de la section méridienne en y faisant y = O, soit

$$[\,x^2 + z^2 - (r^2 + b^2 - a^2)\,]^2 - 4\,a^2\,(x^2 - b^2) = \mathrm{O}$$

Il est d'emblée évident que la section méridienne, courbe du 4e degré, n'est plus une ellipse ; il y a donc lieu d'examiner celle-ci de plus près, pour voir dans quelle mesure elle convient pour les surfaces toriques en lunetterie.

Recourons ici encore aux procédés simples et précis de la géométrie descriptive ; la figure 7 en donne l'épure ; la section méridienne située dans le plan de profil P P′ est rabattue à droite. Elle prend la forme d'un secteur ménisque. L'arc concave (1) est engendré par la petite portion de cercle avec A comme sommet, tandis que l'arc convexe (2) est engendré par la portion de cercle avec B comme sommet.

Faisons d'abord une vérification importante. En appliquant à l'équation de la section méridienne la formule donnant le rayon de coubure pour les sommets A et B on trouve dans le 1er cas en tenant compte

que $\mathrm{OD} = \mathrm{b} = \dfrac{r - a}{\mathrm{tg}\ \alpha}$

$$R_{\mathrm{A}} = \frac{D}{2 \sin \alpha} = \mathrm{AO'_1}$$

dans le second cas (avec $\mathrm{OD} = b = \dfrac{r + a}{\mathrm{tg}\ \beta}$

$$R_{\mathrm{B}} = \frac{D}{2 \sin \beta} = \mathrm{BO'_2}$$

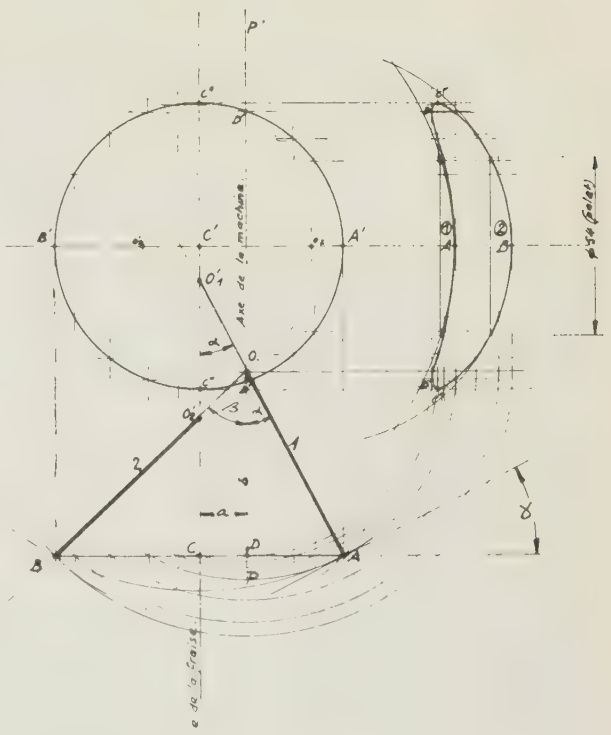

Fig. 7.

Si dans une épure faite à l'échelle 5/1 nous reportons ces 2 rayons de courbure aux points A et B de la section méridienne rabattue, et y traçons les arcs des cercles correspondants, nous constatons que l'arc concave (A) de la section coïncide au centre avec l'arc de cercle sur une notable longueur ; vers l'extrémité les courbes se séparent assez brusquement, par suite de l'inflexion et du brusque changement de la courbure. Cette déformation abrupte vers les bords sera d'autant plus sensible et néfaste que le verre aura un plus grand diamètre.

Pour l'arc convexe (B) au contraire la coïncidence parfaite est obtenue sur une plus grande longueur d'arc, tandis que la séparation des courbes vers l'extrémité de la section, tout en n'étant qu'une fraction des écarts précédents, est régulière et progressive, donc bien plus favorable à une correction systématique. Ces résultats sont nettement illustrés dans le diagramme et les tableaux de la figure 8. Les nombres $\Delta$ A et $\Delta$ B donnent les écarts entre les abscisses des points correspondant du cercle à courbure constante du sommet et de la courbe méridienne taillée par le diamant. La courbure en $\Delta$ A est de 7 dioptries, celle en $\Delta$ B de 10 dioptries.

Remarquons encore que les déformations sont dans les 2 cas de sens opposés ; une surface convexe du type A a les bords brusquement relevés, tandis que le convexe type B a les bords légèrement et progressivement rabattus. L'inverse se produit pour les surfaces concaves. Ces considérations concernent uniquement les méridiens donnés par l'épure, c'est-à-

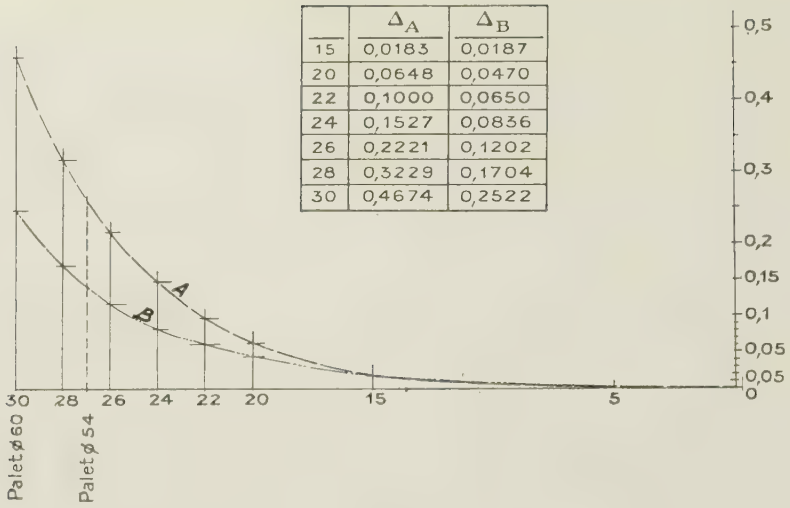


| | $\Delta_A$ | $\Delta_B$ |
|---|---|---|
| 15 | 0,0183 | 0,0187 |
| 20 | 0,0648 | 0,0470 |
| 22 | 0,1000 | 0,0650 |
| 24 | 0,1527 | 0,0836 |
| 26 | 0,2221 | 0,1202 |
| 28 | 0,3229 | 0,1704 |
| 30 | 0,4674 | 0,2522 |

Fig. 8.

dire les méridiens contenant l'axe de révolution. Dans la direction perpendiculaire nous trouvons des sections circulaires parfaites, puisque ce sont (par définition) les cercles parallèles dans des plans perpendiculaires à l'axe de révolution. Pour compléter les considérations géométriques ci-dessus, ajoutons que dans le premier cas (section 1.A.) $R_A = AO'_1$ est le rayon du méridien de base, tandis que $AO = R_C$ est le rayon du méridien du cylindre qui décrit un cercle exact. Dans le second cas (section 2.B.) $R_B = BO'_2$ est au contraire le rayon du méridien cylindre, tandis que BO, donnant la section circulaire exacte, est le rayon de base. Dans la pratique on inverse le mouvement qui servit de base aux calculs ci-dessus. Au lieu de faire décrire par le cercle de la fraise le mouvement de rotation autour de l'axe de révolution, on immobilise au contraire ce cercle ; par contre le verre porté par un chariot peut coulisser le long d'une table qui pivote autour de l'axe O. Mathématiquement et cinématiquement le résultat est le même. On se rend immédiatement compte que si le chariot porte-verre est situé entre l'axe O et la fraise, le cercle tranchant taillera une surface convexe dans le verre ; si au contraire le centre de rotation est déporté du côté opposé au chariot porte-verre par rapport à la fraise, les surfaces engendrées sont concaves.

Contrairement à l'usage préconisé par les constructeurs, il y aurait très nettement avantage à générer les surfaces toriques pour l'arc (B) extérieur de la section méridienne ; cette méthode qui donne des surfaces nettement moins déformées, exige bien entendu, une fraise diamantée présentant un plus profond dégagement intérieur.

*Manuscrit reçu le 15 août 1956.*

# Corrections of interference thickness measurements of thin films on account of boundary reflections

Per J. Lindberg *

Royal Institute of Technology, Stockholm

Summary. — *Multiple-beam interferences show a remarkable effect owing to boundary reflections when a transparent film is interposed between the interferometer flats. Similar conditions occur in all interferometric thickness measurements of transparent films. The phase shift so caused is calculated and represented in diagrams with rolling circles. Measurements were made with multiple-beam interference on zinc sulphide films deposited on silver, and the results agreed satisfactorily with the calculations. If the boundary reflections are neglected in the case of multiple-beam interference the error in the determination of the film thickness is at most about $\lambda/2\pi$, even if the difference in refractive index is small. The consequences of this are considered for the interferometric measurement of biological specimens.*

Sommaire. — *Les interférences à ondes multiples donnent lieu à un effet remarquable propre aux réflexions limites quand une lame transparente est interposée entre les plans de l'interféromètre. Ces phénomènes se produisent dans toutes les mesures interférométriques d'épaisseur de lames minces. Le changement de phase qui en résulte est calculé et représenté sur des diagrammes cycloïdaux. Les mesures ont été effectuées par interférences à ondes multiples sur des couches de sulfure de zinc sur argent et les résultats concordent de façon satisfaisante avec les calculs. Si les réflexions limites étaient négligées dans le cas des interférences à ondes multiples, l'erreur dans la détermination de l'épaisseur du film serait au plus égale à $\lambda/2\pi$ même si la différence des indices de réfraction est petite.*

*L'application aux interféromètres pour mesures biologiques est étudiée.*

Zusammenfassung. — *Mehrstrahlinterferenzen weisen wegen der Reflexionen an den Grenzflächen einen beachtenswerten Effekt auf, wenn ein durchsichtiger Film zwischen die Interferometeroberflächen gebracht wird. Ähnliche Verhältnisse treten bei allen interferometrischen Dickenmessungen durchsichtiger Filme ein. Der entstehende Phasensprung wird berechnet und in Diagrammen mit rollenden Kreisen dargestellt. Messungen mit Mehrstrahlinterferenzen wurden an Zinksulfidfilmen vorgenommen, die auf Silber aufgedampft sind. Das Resultat stimmt mit den Berechnungen zufriedenstellend überein. Wenn man die Reflexionen an den Grenzflächen im Fall der Mehrstrahlinterferenzen vernachlässigt, so ist der Fehler bei der Bestimmung der Filmdicke höchstens ungefähr $\lambda/2\pi$, auch wenn die Brechzahldifferenz klein ist. Die Ergebnisse haben Bedeutung für interferometrische Messungen an biologischen Präparaten.*

I. **Introduction**. — The method developed by Tolansky [1] and others to measure small phase shifts with multiple-beam interference gives a very high accuracy in measurements of surface smoothness, the thickness of deposited layers and the height of steps in crystal surfaces. The accuracy and the sensitivity of these measurements have been increased by giving the interferometer flats a reflectivity very close to 100 per cent and a minimum of absorption [2]. Suggestions have been made among others by Merton [3], Hallén and Ingelstam [4], Nomarski [5] and Cagnet [6] to utilize this accuracy to measure the optical thickness of thin films and biological specimens by inserting them between the two interferometer flats. The fringe displacement so obtained should indicate the difference in optical thickness between the film and an equally thick film of the surrounding medium **. When realizing these ideas it was found by Glauert [7] and by the author that the fringes did not only indicate the variations of the film thickness, but were also changed in shape resembling wavelines or zigzags. In figure 1 are shown three interferograms of the same portion of a collodium film in air with different fringe spacing. The lower part in each contains Newton fringes and shows how these continue into the region between two mirrors constituting a multiple-beam interferometer, where they modulate the fringes. The zigzag modulation period equals the spacing of the Newton fringes. Polster [8] has discussed the case with deposited films. The zigzag effect has been explained analytically by Hunter and Nabarro [9] who have pointed out its importance for the interpretation of microbiological interferograms. They supposed that the effect which is caused by reflections at the boundary surfaces of the film should be of negligible influence when the difference in refractive index is small, but the present calculations show that, by neglecting the reflections, the error in the determination of the film thickness from the fringe displacement is about constant and independent of the refractive index.

For the sake of completeness we shall also consider other cases than that of the multiple-beam interferometer.

II. **Films illuminated from one side only**. — The thickness of a film can be measured by inserting it in one of the branches of a Jamin interferometer or over one of the two slits in a Young interferometer. The fringe displacement so obtained is due to the delay of the light wave passing through the film. This delay or phase shift is mainly due to the difference in optical path between the film and an equally thick " air film ". To obtain the exact value of the phase shift, however, a correction must be introduced caused by the internal reflections inside the film.

(*) Now at the Research Institute of National Defence, Stockholm 80, Sweden.

(**) Note added in proof : The method is also suggested by M. Françon, *Handbuch der Physik*, **24**, 250, Berlin, 1956. No corrections are applicated.

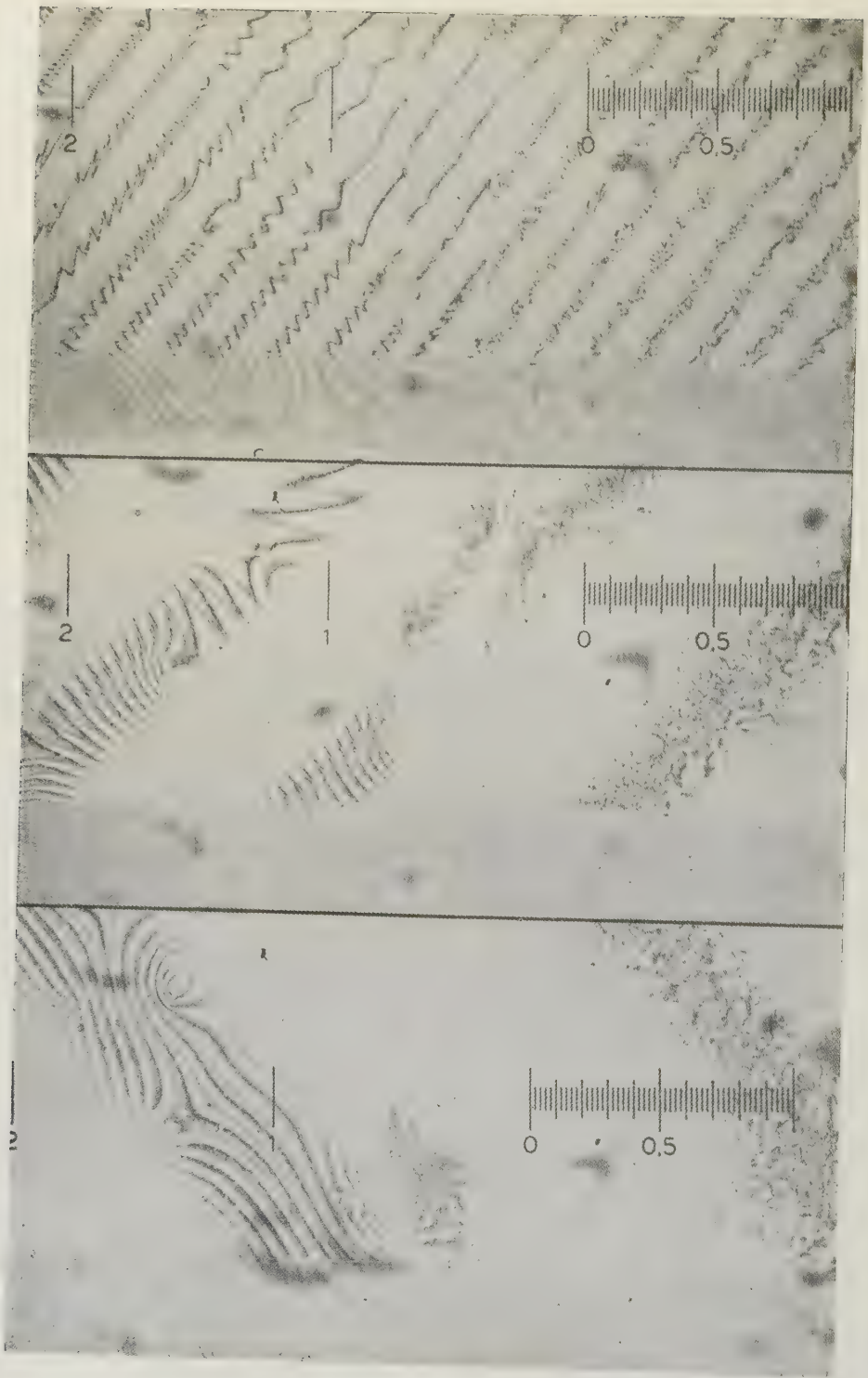


Fig. 1. — Three interferograms with different fringe spacing of the same collodion film formed as a step wedge. Newton fringes seen in the lower part of each modulate the multiples-beam interference fringes into zigzags.

The complex transmission coefficient of a film is

$$t = \frac{(1 - r^2)\, e^{i knx}}{1 - r^2\, e^{2 i knx}} \tag{1}$$

$x$ is the thickness of the film and $r$ is the Fresnel reflection coefficient of the boundary surfaces of the film which is equal to $(n - 1)/(n + 1)$. Here $n$ is the refractive index of the film relative to its surrounding

medium, and $k = 2\pi/\lambda$, where $\lambda$ is the wavelength in the surrounding medium. Since we are not dealing with any variations with time, we choose

$$e^{i(knx - \omega t)}$$

as the wave function instead of its complex conjugate, thus taking the positive sign in the length dependent factor.

The phase shift $\Phi$ between the wave transmitted through the film and the reference wave is the difference between the argument of the corresponding wave functions, *i. e.*, using (1)

$$(2) \quad \Phi = \arg t - \arg e^{ikx} = k(n-1)x + \\ + \arg (1 - r^2 e^{-2ikx}).$$

The fringe displacement observed by viewing the film through the eyepiece of the JAMIN interferometer, or measured in the YOUNG double slit interferometer is proportional to $\Phi$. The constant of proportionality is determined by the geometry of the interferometer in such a way that one fringe corresponds to 360°. A small angle of tilt of the film does not change the result.

If the film is thick the main term of (2) is $k(n-1)x$. The remaining term regarded as a function of $x$ is periodic and can be both positive and negative. It appears as a correction term when $x$ is evaluated from the measured phase shift $\Phi$. We call it a phase correction and denote it by $\varphi$.

$\varphi$ can be represented in the circle diagram in figure 2 a, in which the point A lies at unit distance from O, the centre of a circle of radius $r^2$. The length AB′ equals $(1 + r^2)\,|t|$, which can be proved by the chord rule.

To be able to incorporate the main term $k(n-1)x$ into a circle diagram we first split $\varphi$ into two terms

$$(3) \; \varphi = \arg (1 - r^2 e^{-2ikx}) = \arg (1 - r\, e^{-ikx}) + \\ + \arg (1 + r\, e^{-ikx}).$$

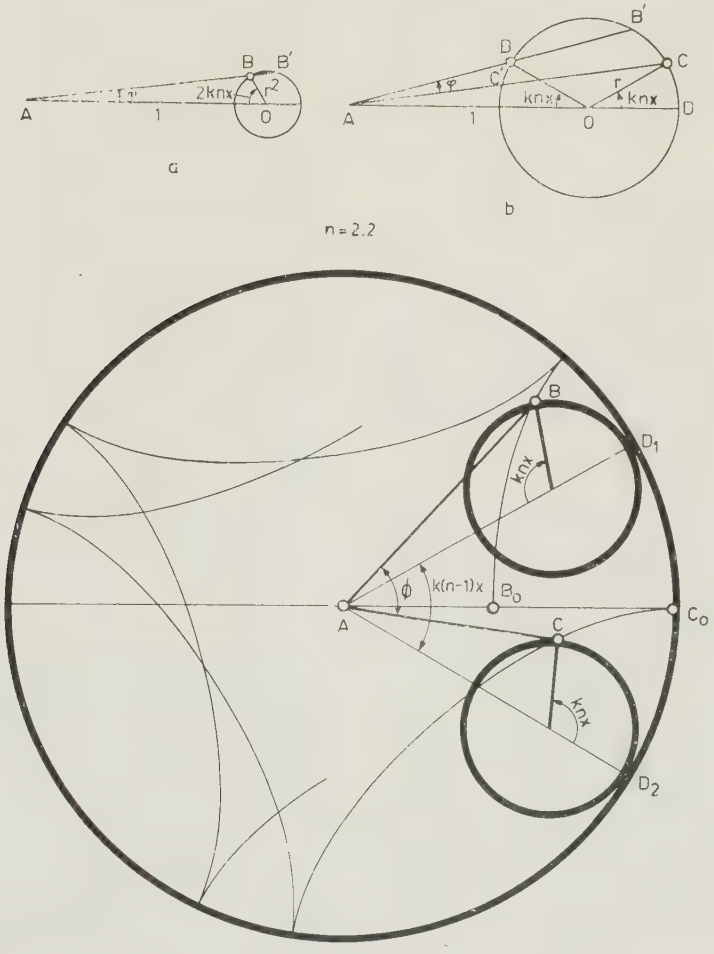


FIG. 2. — a and b. Circle diagrams for the phase shift correction due to boundary reflections in a film illuminated from one side.

c. Rolling-circle diagram for the whole phase shift.

Accordingly the phase correction can be obtained in a diagram with a circle of radius $r$ as is shown in figure 2b. The points B and C rotate in opposite directions when $x$ increases. The distance AO is of unit length. By the chord rule it is easily proved that the absolute value of the transmission coefficient equals the ratio between the lengths

$$\frac{AB'}{AC} = \frac{AC'}{AB} = |t|.$$

If two circles of radius $r$ roll on equal paths $rknx$ on the incide of a larger circle of radius $1 + r$ in opposite directions according to figure 2c, then the angle $D_1AD_2$ is equal to

$$\frac{2\,rknx}{1+r} = k(n-1)\,x.$$

B and C move along hypocycloids from their starting points $B_0$ and $C_0$. The angle BAC is the phase shift $\Phi$ now including the main term as well as the phase correction. If the reflection coefficient $r$ is small, *e. g.* when $n$ is close to unity the two correspondingly small circles have to make a large number of revolutions for $\Phi$ to amount to a certain value. The diagram does not repeat in like manner after one rotation round A unless $1/r$ is an integer.

III. **Films illuminated from both sides.** — Hitherto we have analysed the case when only those beams have interfered which have suffered an even number of reflections at the boundary surfaces of the film. The phase correction was seen to be of the order of magnitude of $r^2$. In some applications, however, the first order reflections also interfere, thus causing a phase correction of the order of magnitude of $r$. This is the case in multiple-beam interferometry of thin films and in certain measurements with the Michelson interferometer. The characteristic feature of these cases is that the film is placed near and parallel to a highly reflecting mirror. The field of view in the interferometer is similar to that in the Jamin interferometer, but the phase shift and the fringe displacement caused by the interposed film is different. This is due to the first order reflections at the two surfaces of the film, which occur since the film is illuminated from both sides.

The combination of the film and the highly reflecting mirror can be regarded as one reflecting system, being the same for the Michelson and the multiple-beam interferometer. The phase shift measurement is then made on this system, no matter which instrument is being used. By so doing we need not analyse all the repeated reflections that take place in a multiple-beam interferometer, as is done by Hunter and Nabarro [9]. All these reflections suffer the same phase shift from the phase object as the single beam in the Michelson interferometer, and the fringe displacement in both cases is proportional to this phase shift. Consequently we need only treat the latter case. This way of looking at interferometrical problems is used by Schulz and Scheibner [10].

The principle in the present problem is illustrated in figure 3a, where the figures to the left indicate the different optical media. The upper mirror used in multiple-beam interferometry is omitted since it does not influence the phase shift. We consider a light wave of unit amplitude falling onto the film from above. After single and multiple reflections and transmissions at the film surfaces and the mirror the wave leaves the film upwards. This is indicated as a beam emerging at A. The reference wave of unit amplitude emerges at B at the same height from the mirror. The

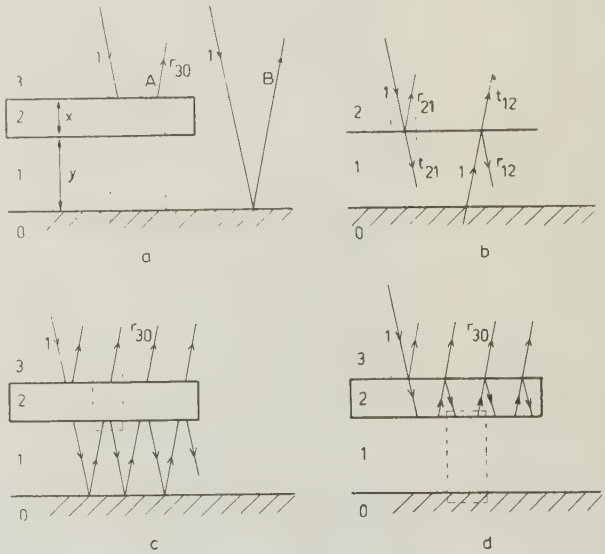


Fig. 3. — a. Principle of thickness measurement of a film illuminated in the interferometer from both sides.

b. Definition of reflection and transmission coefficients used in the formulae.

c and d. Two different ways of summing multiple reflections.

phase difference between the waves at A and B causes the fringe displacement. The wave function at A is the complex reflection coefficient for the two-layer (1, 2) which we denote $r_{30}$. We use the common notation for reflection and transmission coefficients defined in figure 3 b. The wave function at B is

$$r_{10}\,e^{i(2kx+2ky)} = r_1\,e^{i(2kx+2ky+\alpha)}.$$

$x$ is the film thickness as before and $y$ is the distance between the film and the mirror. $r_{10}$ is the complex reflection coefficient for the highly reflecting mirror. Its absolute value is $r_1$ and its argument is the phase shift at reflection, $\alpha$. The phase shift causing the fringe displacement is consequently

$$(4) \qquad 2\,\Phi = \arg r_{30} - (2\,kx + 2\,ky + \alpha).$$

We write it $2\,\Phi$ since the wave mainly transverses the film twice.

Practically, the meaning of (4) is simply that the

measurement of film thickness is regarded as a measurement of a step in the highly reflecting mirror, the step being optically equivalent to the actual phase shift. This thought is expressed by FREDRIKSE [11], although he did not consider the film reflections. Measurements of real steps are familiar in multiple-beam interferometry. No interference method with monochromatic light at normal incidence is capable of distinguishing a film edge from a real step in the highly reflecting mirror.

To obtain $\Phi$ we must calculate $r_{30}$. Reflection coefficients for multi-layers are calculated with recursion formulae. We do this here in two different ways which are illustrated at the bottom of figure 3. In figure 3c multiple reflections are assumed to take place between the lower mirror and the film. The film is regarded as a boundary surface with reflection and transmission coefficients which are dependent on the film thickness. $r_{30}$ is obtained as the sum of all waves emerging upwards through the film. In figure 3d we sum instead all multiple reflections between the upper film surface and the combination of the lower film surface and the mirror, this combination having coefficients depending of the distance $y$. Following these two lines we arrive at two different formulae for $\Phi$, which of course give identical results. The former formula is suitable for the study of $\Phi$ when $y$ varies and $x$ is constant. The reverse is true for the latter. Although they are elementary there is more work to convert them into each other than to deduce them separately in the way mentioned.

A. *Constant film thickness.* — If the lower mirror in figure 3c is a perfect one, *i. e.* if $r_1$ is unity, $|\, r_{30}\,|$ must also be unity since no energy is absorbed in the film. In this case the vector representation of $r_{30}$ is a circle of unit radius. Such vector diagrams have been constructed by MESSNER [12]. The phase, *i. e.* arg $r_{30}$, is, however, a rather involved function of $x$ and $y$. We shall find that we make only a negligible error in the phase by putting $r_1 = 1$, although the error in $|\, r_{30}\,|$ would be greater.

In figure 3c the summation formula for the total reflection coefficient is

$$(5)\qquad r_{30} = \frac{r_{31} + (t_{31}\, t_{13} - r_{31}\, r_{13})\, r_{10}\, \mathrm{e}^{2\,\mathrm{i}\,ky}}{1 - r_{13}\, r_{10}\, \mathrm{e}^{2\,\mathrm{i}\,ky}},$$

where the indices refer to the four optical media indicated to the left in the figure. This is a general formula for the calculation of multi-layers, since the FRESNEL conditions for the $t$'s and $r$'s need not be satisfied. According to the symmetry of the film

$$t_{31} = t_{13} = t$$

given by (1), and

$$(6)\qquad r_{31} = r_{13} = \frac{-r + r\, \mathrm{e}^{2\mathrm{i}\,knx}}{1 - r^2\, \mathrm{e}^{2\mathrm{i}\,knx}}.$$

The absolute value of $r_{31}$ is

$$(7)\qquad \rho = \frac{2\, r \sin knx}{\sqrt{1 + r^4 - 2\, r^2 \cos 2\, knx}},$$

and from (6) its arguments is obtained as

$$knx + \varphi + \frac{\pi}{2},$$

where $\varphi$ is given by (3). Contrary to the case when the upper reflecting system is a single boundary surface, the factor before the exponential in the numerator of (5) here departs from unity, being instead

$$t_{31}\, t_{13} - r_{31}\, r_{13} = \mathrm{e}^{2\mathrm{i}(knx+\varphi)}.$$

Again introducing $r_1$ we insert all the required quantities into (5) obtaining

$$r_{30} = -r_1\, \mathrm{e}^{\mathrm{i}(2ky+\alpha+2knx+2\varphi)}\, \frac{1 + \frac{\rho}{r_1}\, \mathrm{e}^{-\mathrm{i}\left(2ky+\alpha+knx+\varphi-\frac{\pi}{2}\right)}}{1 + r_1\, \rho\, \mathrm{e}^{\mathrm{i}\left(2ky+\alpha+knx+\varphi-\frac{\pi}{2}\right)}}.$$

Here we apply the mentioned approximation by putting $r_1 = 1$ to simplify the formula. The error so made will be discussed later. The final expression for $\Phi$ is then from (4)

$$(8)\qquad \Phi = k(n-1)\, x + \varphi + \arg\left[1 + \rho\, \mathrm{e}^{-\mathrm{i}\left(2ky+\alpha+knx+\varphi-\frac{\pi}{2}\right)}\right],$$

where $\varphi$ and $\rho$ are determined from (3) and (7).

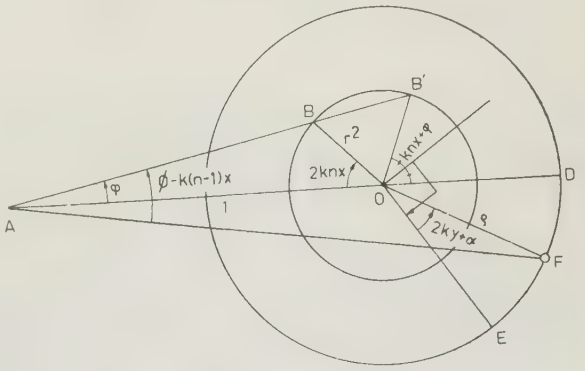


FIG. 4. — Circle diagram for the phase shift correction due to boundary reflections in a film of constant thickness in a multiple-beam or Michelson interferometer.

In (8) the first two terms are identified from (2). The remaining term is of the same structure as $\varphi$, so it can be represented in a circle diagram. We call the last two terms in (8) the phase correction and draw a geometrical construction of it in figure 4. To obtain $\varphi$ we copy figure 2a. Then, concentrically with the circle of radius $r^2$ we draw another one of radius $\rho$. To find the starting point for the running angle $2ky + \alpha$ we notice that the angle B'OD is $2knx + 2\varphi$. Accordingly the bisection of this angle

is rotated 90° clockwise to E, from which the angle $2ky + \alpha$ runs counterclockwise around the circle of radius $\rho$. The angle BAF is the phase correction. When F runs around the circle the phase correction oscillates about its mean value $\varphi$.

Figure 4 and (8) are suitable for the study of the phase shift when a plane parallel film is inserted in the interferometer. $x$ is then constant and if the film is slightly tilted, $y$ varies linearly along the film surface giving rise to zigzagged interference fringes of the type shown by Glauert. These oscillate about the mean line corresponding to the mean phase shift

$$\bar{\Phi} = k\,(n - 1)\,x + \varphi, \tag{9}$$

with an amplitude arcsin $\rho$, which is obtained from figure 4 when FA is tangent to the circle of radius $\rho$. (9) and (2) are identical expressions although they occur in different interferometrical applications.

B. *Variable film thickness.* — In figure 3d we sum multiple reflection between the upper film surface and the combination of the lower film surface and the mirror and obtain

$$r_{30} = \frac{r_{32} + r_{20}(t_{32}\,t_{23} - r_{32}r_{23})\,\mathrm{e}^{2\mathrm{i}knx}}{1 - r_{23}\,r_{20}\,\mathrm{e}^{2\mathrm{i}knx}} = \frac{-r + r_{20}\,\mathrm{e}^{2\mathrm{i}knx}}{1 - r\,r_{20}\,\mathrm{e}^{2\mathrm{i}knx}}. \tag{10}$$

Since the upper reflecting system is a single boundary surface the bracket before the exponential in the numerator is unity. Making the approximation $r_1 = 1$ we also obtain

$$r_{20} = \frac{r + r_1\,\mathrm{e}^{\mathrm{i}(2ky+\alpha)}}{1 + r\,r_1\,\mathrm{e}^{\mathrm{i}(2ky+\alpha)}} = \mathrm{e}^{\mathrm{i}(2ky+\alpha-2\psi)},$$

where

$$\psi = \arg\,[\,1 + r\,\mathrm{e}^{\mathrm{i}(2ky+\alpha)}\,]. \tag{11}$$

Inserting $r_{20}$ into (10) and using (4) we obtain the final expression for the phase shift

$$\Phi = k(n-1)x - \psi + \arg[\,1 - r\,\mathrm{e}^{-\mathrm{i}(2knx+2ky+\alpha-2\psi)}\,], \tag{12}$$

where $\psi$ is determined from (11). (12) and (8) are two identical formulae for $\Phi$. The detailed algebraical proof of this is of no interest here.

The last two terms in (12) are the phase correction. Its representation in a circle diagram is shown in figure 5a. $\psi$ is first constructed from the constant angle $2\,ky + \alpha$. Since the angle B′OA is $2\,ky + \alpha - 2\,\psi$, the point B′ becomes the starting point for the running angle $2\,knx$. The phase correction is the angle CAB. Its mean value is $-\psi$. If in figure 4 $knx$ is a whole multiple of $\pi$, $\varphi$ vanishes. Then, since $\rho$ also vanishes, the phase correction is zero whatever the value of $2\,ky + \alpha$. In figure 5a this situation corresponds to C and B′ coinciding, also leading to a zero value of the phase correction, whatever the value of $2\,ky + \alpha$.

The whole phase shift given by (12) can be represented by means of a rolling circle. Figure 5b shows how the circle from figure 5a rolls on the inside of a larger circle of radius $1 + r$. The contact point moves the arc $D_0D$ along the larger circle when $x$ increases from zero. This arc equals the arc B′C, which is $2knxr$. Since $2\,ky + \alpha$ and thereby $\psi$ is constant during the rolling, the angle $BAB_0$ equals $DAD_0$ which is

$$\frac{2\,knxr}{1 + r} = k(n - 1)\,x.$$

Starting with $x = 0$, *i. e.* with the points C and B′ coinciding at $C_0$, B′ moves along a circle, not drawn in the figure, and C which is fixed to the rolling circle traces a hypocycloid. The angle $CAC_0$ is the phase shift including the phase correction as well as the term $k(n - 1)\,x$. The diagram does not repeat in like manner after a complete revolution round A unless $1/r$ is an integer.

Figure 5b and formula (12) are suitable for the evaluation of interferograms of films of unknown thickness and with the lower surface parallel to the interferometer mirror. An example of this is the measurement of the thickness of a transparent film deposited onto a silver mirror. In this case $y = 0$ and $\alpha$ is the phase shift on reflection onto silver in air or in the immersion medium, despite the fact that the film is in optical contact with the silver. Knowing $\alpha$ and the refractive index of the film we are able to obtain the thickness from the measured fringe displacement by means of (12).

C. *The error by assuming* $r_1 = 1$. — In the deduction of (8) and (12) the departure of $r_1$ from unity has been neglected in functions of the type

$$\frac{1 + r_1\,\rho\,\mathrm{e}^{\mathrm{i}\beta}}{1 + \dfrac{\rho}{r_1}\,\mathrm{e}^{-\mathrm{i}\beta}}.$$

Since we have been mainly interested in the argument of such functions we write this

$$\arg\,(1 + r_1\,\rho\,\mathrm{e}^{\mathrm{i}\beta}) + \arg\,(1 + \frac{\rho}{r_1}\,\mathrm{e}^{\mathrm{i}\beta}),$$

and represent it in a diagram by means of two circles of radius $r_1\rho$ and $\rho/r_1$ in figure 5c. Instead of the arithmetical mean of the two arg-functions we used in the formulae the arg-function obtained from a circle of radius $\rho$, which is the geometrical mean radius of the two proper circles. This would of course be allowed if $r_1$ were unity, but if not, the error so made can be shown to be of the magnitude of

$$\delta = \frac{1}{2}\,(1 - r_1)^2\,\rho.$$

Taking $\rho$ to be as great as 0.4, which is its maximum value for $n = 1.5$, and the reflectivity of the mirror to be as low as 90 per cent, the error amounts to

$$\delta = 0.0005 \text{ radian} = \frac{\lambda}{12\,000} \text{ units of length.}$$

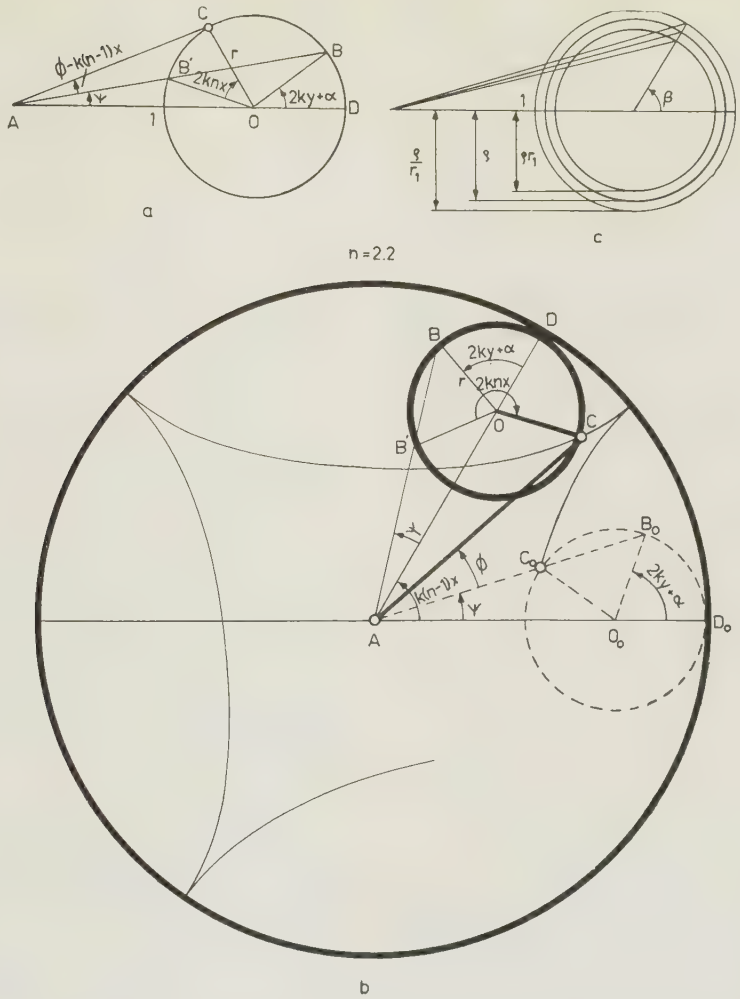


FIG. 5. — a. Circle diagram for the same phase shift correction as in figure 4, but for variable film thickness.

b. Rolling-circle diagram for the whole phase shift with variable film thickness.

c. Diagram showing the error made in the formulae by putting $r_1 = 1$.

This error is hardly detectable by means of interferometry, so we were justified in the approximation putting $r_1 = 1$.

IV. **The phase shift in Cartesian diagram.** — Although figure 2, 4 and 5 give a survey of the phase shift caused by an interposed film in different applications these diagrams are not very convenient for numerical evaluations of measurements. The problem is to determine the number of rotations that the circle has to make for a point on it to reach a certain radius corresponding to the measured phase shift. Therefore we could draw a family of hypocycloids, but more conveniently we plot instead the phase shift $\Phi$ in a Cartesian diagram in figure 6 against the optical film thickness $knx$. The curve denoted I is the phase shift from (2) and is applicable to measurements of films which are illuminated from one side only.

The next formula to be plotted in the diagram is (8). Its first two terms are already shown. If we know nothing about $2ky + \alpha$, we can only say that the remaining term is within $\pm$ arcsin $\rho$ ; $\rho$ depends on $x$ by (7) so the " uncertainty borders " have the equations

$$\Phi_{\substack{\max \\ \min}} = k(n - 1)\, x + \varphi \pm \arcsin \rho.$$

The dashed curves II in figure 6 which is valid for $n = 2.283$ are the uncertainty borders. Since (7) can be written

$$\arcsin \rho = \arg (1 + r\, \mathbf{e}^{ikx}) (1 - r\, \mathbf{e}^{ikx})$$

and since, by (3) $\varphi$ is given in terms of similar functions, the equations of the uncertainty borders can be transformed into

$$(13) \quad \Phi_{\substack{\max \\ \min}} = k(n - 1)\, x + 2 \arg (1 \mp r\, \mathbf{e}^{-ikx}).$$

The Φ-curves for various $2ky+\alpha$ one of which is plotted and denoted III in figure 6 are all of the same shape and amplitude and lie all within the borders II given by (13), which are the envelope of the curves.

In the case of films illuminated from both sides all curves have points with zero slope. At these thicknesses the phase shift is not sensitive to a variation in the film thickness. This insensitivity occurs in figure 5b when the point C touches the larger circle. Consequently there are only some regions of thickness to which multiple-beam interferometry is applicable and the position of these regions depends periodically on $2ky + \alpha$. On the other hand there are regions with at least double sensitivity compared with that of the term $k\,(n - 1)\,x$. This is because the sensitivity

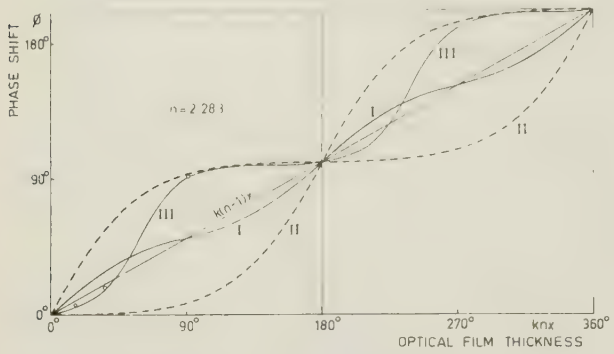


Fig. 6. — Curve I. The phase shift from figure 2 c.
Curve II. The uncertainty borders embracing phase shift curves from figure 5 b.
Curve III. One of these curves with $n = 2.283$, $y = 0$ and $\alpha = 210.45°$.
Small circles indicate measured values for zinc sulphide.

of this term is sometimes overwhelmed and sometimes increased by the phase correction.

In illustrating this we consider (8) for small $knx$. Its first power approximation is

$$\Phi = k(n^2 - 1)\,x\,\cos^2\left(ky + \frac{\alpha}{2}\right). \tag{14}$$

Consequently the interference fringes with extremely thin films oscillate between zero displacement and a displacement corresponding to the phase shift $k(n^2 - 1)\,x$, which is $n + 1$ times $k\,(n - 1)\,x$.

V. **Measurements on zinc sulphide films.** — A " staircase " of zinc sulphide was deposited by evaporation on a opaque silver mirror. The optical thickness of each layer was roughly controlled during the deposition by measuring the reflectivity of a piece of clear glass placed near the target at about the same distance from the evaporation source.

Thickness measurements were made with multiple-beam interference to check formula (8). The curve thereby obtained was intended to be used for other determinations of film thickness es from measured fringe displacements without depositing an extra silver layer. The latter method is used by Tolansky. The fringe displacement was compared with that obtained in the same interferometer after the staircase and its surroundings were covered with an opaque layer of silver. The fringe displacement in the latter case is due only to the real thickness of the zinc sulphide, provided the silver layer is equally thick whether deposited on zinc sulphide or silver. This question is studied by Heavens [13]. A semi-transparent silver mirror of about 5 per cent transmission was placed over the staircase. Two tungsten wires a few microns thick were inserted between the mirrors and adjusted for a suitable fringe spacing. The fringe displacements plotted in figure 6 are the average of three observations for each layer. The errors in the measurements of Φ and $kx$ were less than 0.5°. The best fit to the calculated curve III was obtained for $n = 2.283$. $\alpha$ was taken to 210.45° which is calculated from the optical constants of silver ($n_{Ag} = 0.18 + 3.67\,i$). Using other values of $n$ the departure from the calculated curve will be greater.

The localization of the phase shift curve within the dashed borders in figure 6 is wholly determined by the quantity $2ky + \alpha$. When the optical thickness is within about one half wavelength, the influence on Φ of $2ky + \alpha$ is as great as that of $knx$. The measurements and the curve show that the same experimental errors are to be expected whether the method is used to determine $\alpha$ when $x$ is known or to determine $x$ when $\alpha$ is known.

VI. **Errors by neglecting the boundary reflections.** — By neglecting the reflections at the surfaces of the film, the formula for the phase shift is

$$\Phi = k\,(n - 1)\,x, \tag{15}$$

assuming that $n$ is close to unity and $r$ small. This is the formula commonly used by microscopists. The error in this simplification is obvious from the preceding sections. There are, however, cases when the reflections should be neglected for other reasons than the smallness of $r$. They will be discussed later.

In all cases when the film is illuminated only from one side the phase shift is given by (2). If the reflections are neglected, *i. e.* using (15) instead of (2) for the determination of $x$, the maximum value of the phase correction must be assumed as the possible error in the measured phase shift. Solving for $x$ under these conditions gives an error in film thickness amounting to

$$\delta_1 x = \frac{\arcsin r^2}{k\,|\,n - 1\,|} = \frac{\lambda}{2\pi}\,\frac{\arcsin\left(\dfrac{n-1}{n+1}\right)^2}{|\,n - 1\,|}. \tag{16}$$

$\delta_1 x$ is plotted in figure 7 against the relative refractive index $n$. It should be remembered that $\lambda$ is the wave length not in vacuo, but in the medium surrounding the film, so $n$-values less than unity are possible. They cause a negative phase shift. $\delta_1 x$ vanishes when $n$ approaches unity.

Next we consider the film inserted between two mirrors in a multiple-beam interferometer or into a

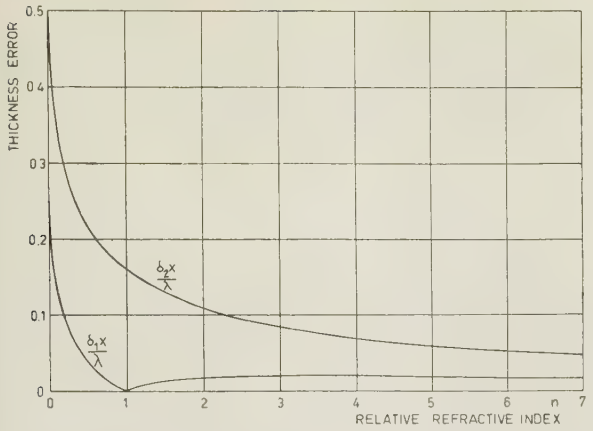


FIG. 7. — Errors in film thickness made by neglecting boundary reflections *versus* refractive index.
$\delta_1 x$ applies to films illuminated from one side only.
$\delta_2 x$ applies to films illuminated from both sides.

MICHELSON interferometer close to one of its mirrors. When the plane parallel film is slightly tilted, we have seen that the fringes oscillate. If the film is large enough to embrace several modulation periods of a fringe the mean fringe displacement can be measured in the interferogram and the film thickness be determined by means of (9). Since this is the same formula as (2) the possible error made by neglecting the reflections in this case is also $\delta_1 x$ given by (16).

If only a limited area of the film is available for interferometric measurements it is necessary to adjust the interferometer spacing, so that a fringe appears just at the spot where the film is situated. $\Phi$ can then be measured exactly, but if there is no information about $y$, the maximum error is the whole phase correction. Its greatest value is 2 arcsin $r$, which is the greatest height from the straight line $k(n-1)\,x$ in figure 6 to the uncertainty border. It can also be seen from figure 5a as the greatest value of the angle BAC. The maximum error in the determination of $x$ is accordingly

$$(17) \quad \delta_2 x = \frac{2 \arcsin r}{k(n-1)} = \frac{\lambda}{\pi} \frac{\arcsin \dfrac{n-1}{n+1}}{n-1} .$$

$\delta_2 x$ is plotted in figure 7. Unlike $\delta_1 x$ it does not vanish when $n$ approaches unity. It is considerably greater than $\delta_1 x$.

Sometimes the boundary surfaces of a film are so rough and curved that the reflections from them are dispersed and arrive outside the microscope lens. The proper formula for the phase shift is then (15). The loss of the reflections causes a lower transmission of the film leading to less sharp fringes, but their position is not affected. The dispersing angles can sometimes be determined from the interferogram, and if they are of such magnitude that the reflections are not collected by the lens their influence can be neglected. If on the other hand the film is found to be nearly plane parallel the error given by (17) must be considered. Even if only one of the boundary surfaces of the film is plane, reflections arise causing a phase correction. When only the upper film surface is plane and gives collimated reflections, the phase shift is

$$\Phi_U = k(n-1)\,x - \arg\left[1 + r\,e^{i(2ky+\alpha)}\right].$$

When only the lower surface is plane, the phase shift is

$$\Phi_L = k(n-1)\,x - \arg\left[1 - r\,e^{i(2ky+\alpha+2knx)}\right].$$

In both cases the maximum phase correction is arcsin $r$, so the uncertainty in the determination of $x$ is half the value given by (17), if the boundary reflections are neglected.

VII. **Biological specimens.** — If a biological section is interposed between the mirrors of a multiple-beam interferometer the fringes are changed in a very irre-

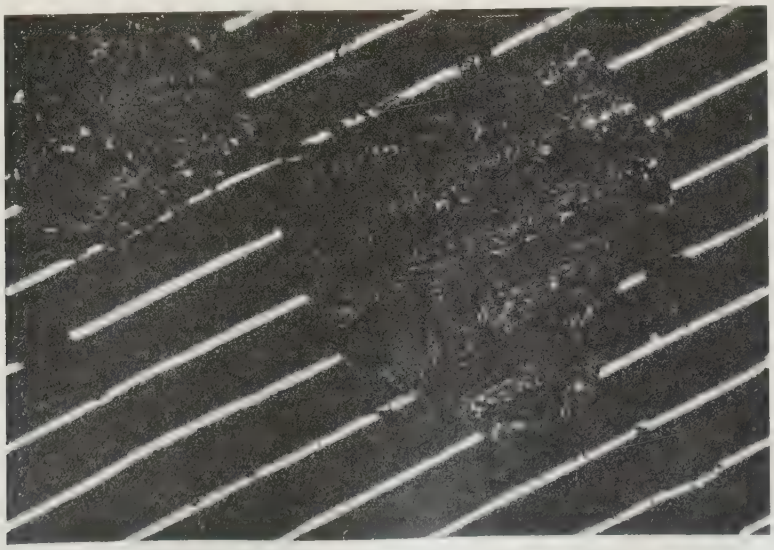

FIG. 8. — Multiple-beam interferogram of cell section embedded in glycerine.

gular way since the specimen is no longer a plane parallel film. Figure 8 is a multiple-beam interferogram of a section of cell structure embedded in glycerine, seen in transmission. The fringe displacements indicate not only the variation of $x$ over the specimen but also the variation of $y$ in a complicated mixture. Also the refractive index may vary over the specimen or even be indefinable, since the immersion liquid may have penetrated into the structure of the specimen.

When the specimen resembles a homogenous film with well defined refractive index its thickness can be obtained from an interferogram within certain limits of error. Since it is very difficult to distinguish the phase shift caused by the $x$-variation from that caused by the $y$-variation the maximum error in film thickness is $\delta_2 x$ given by (17), if the measurement is made at a single spot of the specimen. Often the relative refractive index is near unity, so the maximum error amounts to

$$\delta x = \frac{\lambda}{2\pi} \tag{18}$$

If the thickness of the specimen is more constant and if a rather large piece of it can be mapped it is possible to find the central line in the fringe. The error is then smaller than that given by (18), which, however, in many cases is sufficiently small for thickness measurements of microscopical specimens.

References

[1] S. Tolansky, *Multiple Beam Interferometry of Surfaces and Films*, Clarendon Press, Oxford, 1948.
[2] J. A. Belk, S. Tolansky and D. Turnbull, *J. O. S. A.*, **44**, 1954, 5.
[3] Sir Thomas Merton, *Proc. Roy. Soc.* **A 189**, 1947, 309 ; **A 191**, 1947, 1.
[4] O. Hallén and E. Ingelstam, *Exper. Cell Research* **3**, n° 1, 1952.
[5] G. Nomarski, *Contraste de Phase et Contraste par Interférences*, p. 65, Eon Rev. d'Opt. Paris, 1952.
[6] M. Cagnet, *Rev. Opt.*, **33**, 1954, 1, 113, 229.
[7] Audrey M. Glauert, *Nature*, **168**, 1951, 861.
[8] H. P. Polster, *J. O. S. A.*, **39**, 1949, 1038.
[9] S. C. Hunter and F. R. N. Nabarro, *Phil. Mag.* **43**, 1952, 538.
[10] L. G. Schulz and E. J. Scheibner, *J. O. S. A.* **40**, 1950, 761.
[11] A. M. Fredrikse, *Acta Brev. Neerl. Physiol.* **3**, 1933, 8.
[12] R. Messner, *Feinwerktechnik* **57**, 1953, 297.
[13] O. S. Heavens, *Proc. Phys. Soc.* **B64**, 1951, 419.

*Manuscrit reçu le 7 mai 1956.*

## Information

### Visual Problems of Colour

A Symposium on Visual Problems of Colour will be held at the National Physical Laboratory, Teddington, Middlesex, on 23rd, 24th and 25th September, 1957.

The aspects of the subject to be covered include visual pigments, brightness and colour matching, normal and defective colour vision, subjective colour measurement, electrophysiological aspects of vision and Colour Theories ; about 35 papers will be presented.

Attendance will be by invitation and those interested in being present are requested to write to the Director of the Laboratory.

# Rapid light adaptation of localised areas of the extra-foveal retina

F. J. J. Clarke
Technical Optics Section, Imperial College, London.

Summary. — *The subjective disappearance of peripherally fixated objects has usually been regarded merely as an obstacle to satisfactory observation. The course of local adaptation of a stimulus subtending 40 × 80 minutes of arc on a dark ground has been investigated for the dark adapted extra-foveal retina under conditions of steady fixation, with variation of intensity, wavelength and eccentricity, and for several observers. A time delay of a few seconds followed by a rapid reduction of subjective brightness was always found, the subjective image vanishing outside the paracentral region. It appears that the process is characteristic of both rod and cone units. The origin of the effect is discussed.*

Sommaire. — *La disparition subjective des objets en vision périphérique continue n'a été ordinairement considérée que comme un obstacle à une observation satisfaisante. L'adaptation locale du stimulus de 40 × 80 minutes d'arc en fond obscur, dans les conditions d'observation continue et de fixation soutenue, a été étudiée pour la rétine extra-fovéale adaptée à l'obscurité, en faisant varier l'intensité, la longueur d'onde et l'excentrement pour plusieurs observateurs. On trouve toujours un retard de temps de quelques secondes, suivi d'une réduction rapide de brillance, l'image subjective s'évanouissant complètement en dehors de la région parafovéale. Il apparaît que l'effet est caractéristique à la fois des bâtonnets et des cônes. L'origine de l'effet est discutée.*

Zusammenfassung. — *Das subjektive Verschwinden peripherer fixierter Objekte wird gewöhnlich nur als Hindernis einer befriedigenden Beobachtung angesehen. Der Verlauf der lokalen Adaptation bei einem Reiz, dessen Grösse 40 × 80 Winkelminuten war, mit einem dunklen Umfeld und konstanter Fixierung wurden für die dunkel adaptierte (extrafoveale), Netzhaut untersucht. Die Leuchtdichte, Wellenlänge und Exzentrizität wurden für die verschiedenen Beobachter verändert. In allen Fällen wurde ein Zeitverzug von einigen Sekunden gefunden, dem ein schneller Helligkeitsabfall folgte, wobei das subjektive Bild ausserhalb des parazentralen Teils der Netzhaut verschwand. Der Effekt scheint für das Stäbchensystem wie auch für das Zapfensystem charakteristisch zu sein. Die Entstehung des Effektes wird diskutiert.*

**Introduction.** — When a small test patch on a dark ground is projected on to a position in the peripheral retina determined by fixation, it is found that its subjective brightness begins to decrease rapidly after a few seconds, and that with continued fixation the subjective image will vanish. This phenomenon renders any matching against a foveal or extra-foveal comparison patch impracticable, and is one of the reasons why reliable data on peripheral vision is so hard to obtain.

In the most carefully executed studies on the periphery in recent years, namely those of Weale [1-3] and of Moreland [4, 5], precautions had to be taken to prevent this " fading " of the subjective image. The former used two patches for comparison at the same eccentricity, but tangentially separated by a gap sufficiently large to ensure subjective separation ; thus fading caused approximately equal changes for each patch, and in any case, the observer blinked as required (which inhibits the effect). The latter used a flashing technique for both test and foveal comparison patches, whereby the stimuli were presented for half a second at a time with a resting period for partial recovery of 1 1/2 seconds between presentations. With the periphery initially dark adapted, the area stimulated reached a state of dynamic equilibrium after a few flashes. The frequency and length of flash were chosen for observational convenience.

It was decided that in view of the absence of reliable data on the adaptational processes of the periphery, a study of extra-foveal fading would help to throw some light on these processes. Previous work [6-9], in this field is far from complete. The early studies suffered from the limitations of the equipment available, while some of the more modern works are marred by inadequately controlled conditions of adaptation and viewing [8], and by the questionable procedure of using critical fusion frequency as the criterion of subjective brightness [9]. In any case no one has used exit pupils on their equipment to eliminate the effect of pupillary variation. This is an important consideration, since the introduction of intense stimuli on to a dark adapted retina causes a significant pupillary contraction. Reeves [10] showed that the fast phase of the contraction was complete in 5 seconds ; for a stimulus of as little as 100 ml. and a dark-adapted eye, the effective reduction in iris transmission was 0.6 log units, allowing for the Stiles-Crawford effect.

The process of subjective fading is determined by the state of adaptation, the physical nature of the stimulus, the physiology of extra-foveal perception and possibly by psychological effects. Thus results could depend on 9 experimental parameters, i. e. the intensity, physical constitution, size, location and time of exposure of the pre-adapting field ; and the intensity, constitution, size and location of the test stimulus.

A complete investigation would involve the combined variation of all these parameters, an impracticable proposition. The present study is confined to the dark-adapted retina with fixed test and comparison field sizes, the variable parameters being the intensity, constitution and location of the test stimulus.

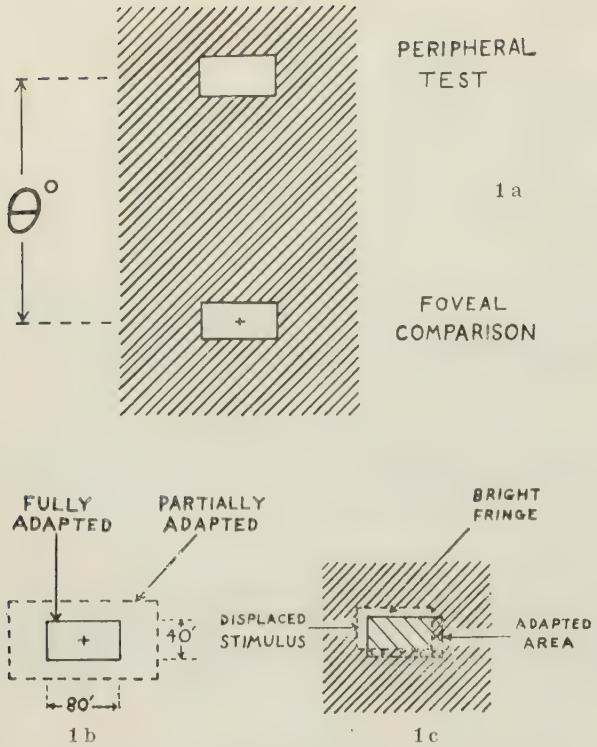


Fig. 1. — (a) Visual field, (b) area of foveal adaptation, (c) the effect with small displacement of test stimulus.

**Method.** — The apparatus used was the Wright colorimeter [ 11 ] modified for peripheral viewing with separation of the visual fields, figure 1 (a), by means of the Moreland attachment [ 4 ] ; this equipment has been adequately described elsewhere. The extra-foveal test and foveal comparison patches were illuminated with monochromatic light of the same wavelength from the two spectra of the colorimeter, the luminances of each being continuously controllable by the observer. The test patch intensity was controlled by means of one of the " primary " wedges of the instrument, the comparison by means of an added auxiliary wedge worked by a crank-handle via a dog-clutch and rack-and-pinion. The auxiliary wedge was always set initially to give maximum transmission for the foveal patch. Attached to the wedgeholder was an arm, to which was pivoted a pen which could rest on a recording drum, the last being steadily rotated at any desired speed by means of an electric gramophone motor, belts and pulleys.

In order to execute successful experiments on peripheral perception it is necessary to position the eye very accurately with respect to the test and comparison beams, the required conditions being that the principal rays of each beam intersect at the centre of the natural pupil, and that the instrumental exit-pupils are close to the natural pupil. These adjustments can be made with considerable precision on this equipment [ 4 ]. Since the contours of physiological equivalence in the retina are approximately ovals concentric with the fovea, it was decided to displace the test patch only radially over the retina for the different observing sessions ; the area of stimulation always lay on the upper meridian of the field of view.

The observational procedure was that, having made the adjustments to set the extra-foveal patch at the desired excentricity θ, figure 1 (a), being adapted only to the moderate level needed for these adjustments, the subject dark adapted for 15 minutes. The subject was then presented with the foveal comparison patch of predetermined luminance and wavelength, which he viewed for three minutes ; during this time he scanned over the whole area of the $40' \times 80'$ patch, the effect being that after three minutes he was fully light adapted over the area of the foveal patch and partly adapted over the surrounding band, whose extent is indicated in figure 1 (b). It has been shown [ 12, 13 ], that the light adaptation of the fovea is complete to within 10 % of the ultimate value after 100 seconds.

At the end of the foveal light adaptation the test patch was presented to the dark adapted periphery in flashes of about 1/2 second or less, about once every five seconds ; this length of flash was just sufficient to obtain a fair impression of brightness but not long enough to produce significant adaptation i. e. the periphery remained effectively in a state of dark adaptation even after 6 or 8 such flashes. The wedge reading was noted after the subject had made a match of brightness against the constant foveal patch, and the observer remained seven minutes in darkness followed by three minutes foveal adaptation before making a second such match. A third match was made by the same technique. Finally the wedge reading of the peripheral stimulus was set to the mean of the three values noted ; thus when this was presented to the dark-adapted periphery the initial subjective brightness was equal to that of the foveal patch as viewed by the light adapted fovea.

After a further seven minutes dark adaptation the recording drum was set in motion with the pen tracing a base line corresponding to the maximum foveal wedge transmission ; since the drum rotated once per minute a sharp noise was heard at this frequency, caused by the pen rising over the securing clamp for the recording paper at time $T = 0$. After a measured three minutes of foveal adaptation the subject fixated on the centre of the dark cross, figure 1 (*a*), about five seconds before the noise was due. On hearing this noise the observer moved a shutter exposing the extra-foveal patch permanently and (while maintaining as steady a fixation as possible) attempted to keep the subjective brightness of the two patches matched by decreasing the luminance of the comparison patch to follow any fading of the test stimulus. Whenever possible fixation was maintained until any rapid changes had ceased, although this involved some strain. Four or five such recorded traces were obtained in an observing session.

It was found that several training sessions were required before an observer became familiar with the

controls and, more important, could learn to maintain a steady fixation for up to twenty seconds. In order top prevent observers from " learning " the crank-movement during previous runs, the phase of the crank was sometimes reversed (using the dogclutch) after the first two runs in a session ; in any case three revolutions were required to increase the wedge density by 1.5 unit. Individuals varied greatly in their inate ability to control their eye movements ; it is only the voluntary movements that can be eliminated by fixation. Some prospective observers were found to have large eye flicks every few seconds, of which they often became aware subjectively, and these were sufficiently large to break the fixation condition.

The angular subtense of the cross was $7 \times 5$ minutes of arc ; if an observer made an extra-foveal patch fade to a low level of brightness by good fixation, and then displaced his point of fixation by a few minutes of arc, this was sufficient to break the fixation condition, for the extra-foveal patch would immediately brighten. The subjective appearance of a $40' \times 80'$ patch at $\theta = 10°$ or larger is that of a small source, and a break of fixation merely results in an instantaneous brightening ; at $\theta$ less than about 10°, some impression of rectangularity exists and a break of fixation causes a bright fringe to appear along one or two sides of the patch. This corresponds to a fresh area of retina being stimulated, figure 1 (c). Thus it was usually quite obvious to the observer at the time of viewing whether he had fixated steadily or not.

**Selected conditions.** — The experiment was performed by observer F. C. at excentricities of 3°, 5°, 10°, 15°, 20°, 30°, and 40°. At all these angles monochromatic light of wavelength $\lambda = 0.53\ \mu$ was used, two levels of subjective brightness, high *H* and low *L*, being employed and kept constant for the initial peripheral sensation, as specified by matching the luminance of foveal patch. The effect of wavelength variation was investigated for values of $\theta = 5°$ (typical of paracentral region) and $\theta = 20°$ (typical of peripheral region), the wavelengths $\lambda$ being 0.65 $\mu$, 0.59 $\mu$, 0.53 $\mu$ and 0.46 $\mu$. At $\theta = 5°$ three values of brightness were used at $\lambda = 0.53\ \mu$ : *H*, *M* and *L*. Since the variation of the fading effect for given $\theta$ and $\lambda$ was to be investigated for change of level, levels *H* and *L* were chosen as high and low as practicable. The low level *L* was about 2 log. units below level *H*, being the lowest at which the subjective contrast for the black cross on the foveal patch was sufficient for fixation after a fading of 1.5 density units on the wedge.

For most experiments a wedge with a useful density range of 1.7 was used ; a high gradient wedge of double this range was acquired, but could only be used for the levels *H* and *M*, for the reason stated above. The photometric data for the various wavelengths and levels are shown in Table 1. The relative sensitivity to monochromatic light for the para-fovea is not very different from the foveal values (Wright [11], Weale [2], Moreland [5]), a small shift of the maximum being reported ; in the periphery however, the longwave sensitivity is heavily depressed (Weale [3], Moreland [5]). This last effect prevented light of 0.65 $\mu$ being used at 20 deg.

Table 1. Photometric data for the pre-adapting values of the foveal comparison field ; these specify the initial brightness levels for the test stimuli.

| Wavelength $\lambda$ microns | Level | Luminance (cd./m.$^2$) | Ret. Illum. (trolands -) |
|---|---|---|---|
| 0.65 $\mu$ | — | $8.0.10^2$ | $2.5.10^3$ |
| 0.65 $\mu$ | *L* | $7.9.10^0$ | $2.4.10^1$ |
| 0.59 $\mu$ | — | $2.1.10^3$ | $6.6.10^3$ |
| 0.53 $\mu$ | *H* | $2.5.10^3$ | $7.9.10^3$ |
| 0.53 $\mu$ | *M* | $2.7.10^2$ | $8.1.10^2$ |
| 0.53 $\mu$ | *L* | $2.9.10^1$ | $9.3.10^1$ |
| 0.46 $\mu$ | — | $2.8.10^1$ | $8.9.10^1$ |

**Observer differences.** — In order to determine whether the results obtained with observer F. C. were typical, several other subjects co-operated in the investigation. For all the confirmatory observations 5 deg. and 20 deg. were used as being typical of the para-central and peripheral regions respectively ; this procedure was justified by the regular transition of fading kinetics shown by observer F. C. Subject J. B. viewed test patches of 0.65 $\mu$ *H*, 0.53 $\mu$ *H*, 0.53 $\mu$ *L* and 0.46 $\mu$ at 5° and of 0.59 $\mu$, 0. 53 $\mu$ *H*, 0.53 $\mu$ *L* and 0.46 $\mu$ at $\theta = 20°$. Observers Mc. F., D. P. and M. D. viewed patches of wavelength 0.53 $\mu$, the first at level *M* the second at levels *H* and *L* and the third at level *H*. In the case of D. P. an anomalous result was consistently obtained at 5 deg., so the experiment was conducted also at 5 deg. in the lower meridian and at 3 deg. in the upper meridian.

All observers were asked to test for after-images with each experimental condition ; this was done by the subject cutting off the peripheral stimulus after it had been made to fade subjectively by fixation.

**Results.** — A mean curve was drawn through the four or five recordings made in a session. For a given observer and conditions, two or more such curves were usually obtained. These appear in figures 2 to 9 for F. C., figure 10 for Mc. F., figures 11 and 12 for J. B., figure 13 for M. D., and figure 14 for D. P. The last mentioned appeared to be anomalous for the whole paracentral region, for he always recorded a typical time delay *T*d (Table 2), followed by a subjective fading so rapid that it could not be followed, even

Table 2. Results for observer DP in the para-central region, showing the length of the latent period preceding the sudden vanishing of the subjective image.

| Observer DP $\lambda = 0.53\ \mu$ | | |
|---|---|---|
| Level | $\theta$ | Mean Delay $T_d$ |
| *H* | 5° | 3.3 secs. |
| *H* | 5° | 2.8 secs. |
| *H* | 5° | 2.8 secs |
| *L* | 5° | 2.9 secs. |

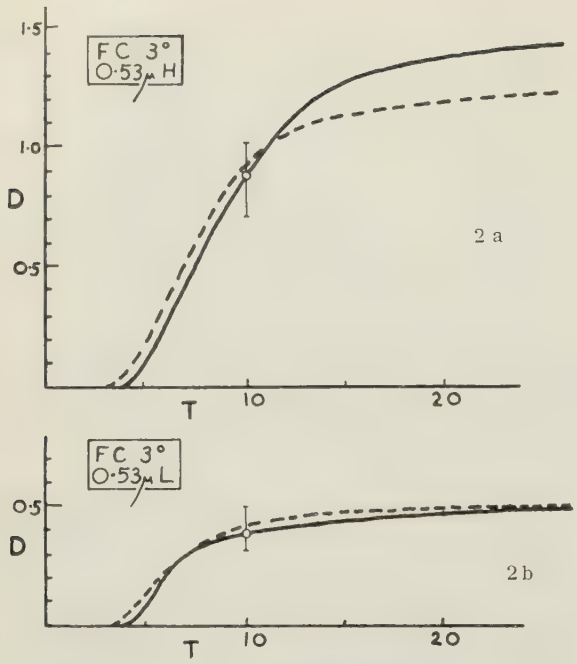


Fig. 2. — Course of extra-foveal fading ; total spread in recorded curves in a session is shown by vertical indicators at $T = 10$ secs.

though the high-gradient wedge enabled 3.0 units of density to be inserted in a half second. In the figures 2 to 14, ordinates represent density $D$ inserted in the foveal comparison beam and abscissae represent time $T$ in seconds ; each set of experimental conditions is specified by a panel containing the observer's initials, the eccentricity θ, the wavelenght λ, and the brightness level. It should be noted that in figure 12 the fading rate increased continuoulsy from time $T$d, and became too fast to follow at the mark shown on each curve.

**Subsidiary binocular experiments.** — It became of interest to study the adaptation at the fovea, to see how the fovea and the extra-fovea compared, and particularly to find if there were a latent period at the former. Since it was clearly impossible to perform the experiment using test and comparison beams projected on to the same retinal area, it was decided to use the binocular matching technique by illuminating the left fovea with the test patch and to retain the comparison patch in the right fovea under the same conditions as before.

The Wright colorimeter was used, in the form for binocular viewing. For the preliminary matches the procedure was (1) binocular dark adaptation, (2) right foveal adaptation to the same levels as before, (3) presentation of left test patch in flashes, with adjustment of the test to match the comparison field brightness. For the recording of the course of adaptation, the procedure was (1) dark adaptation, (2) right foveal light adaptation, (3) simultaneous viewing of the test and comparison fields, with continuous adjustment of the auxiliary wedge to maintain equality of brightness between the two fields.

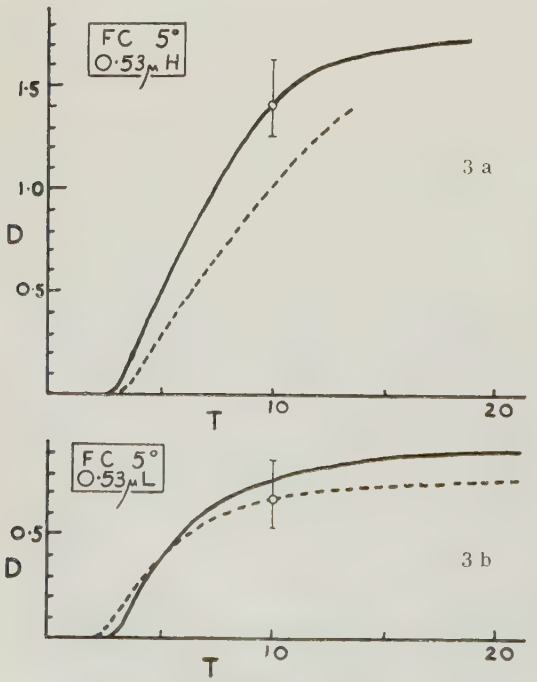


Fig. 3 a b.

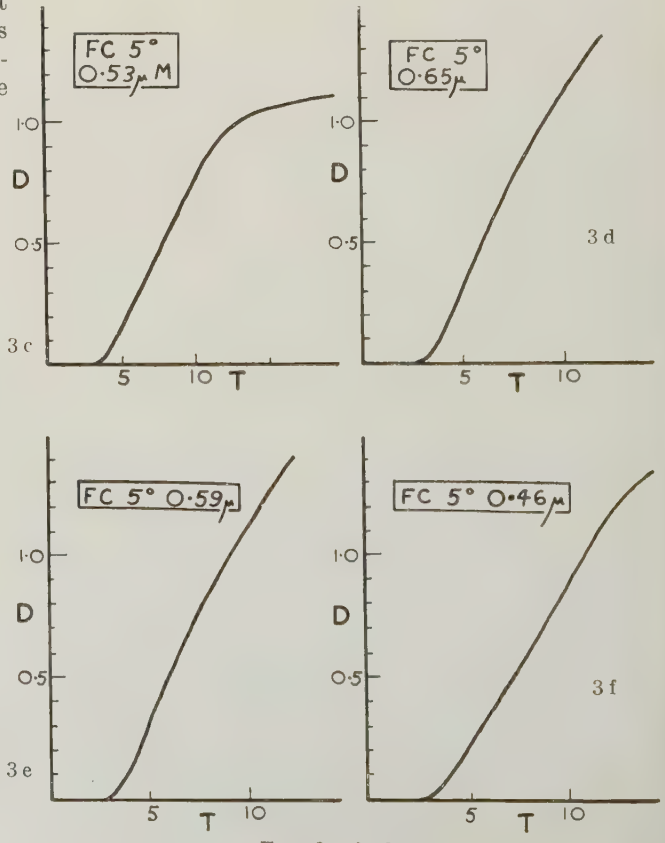


Fig. 3 c d e f.

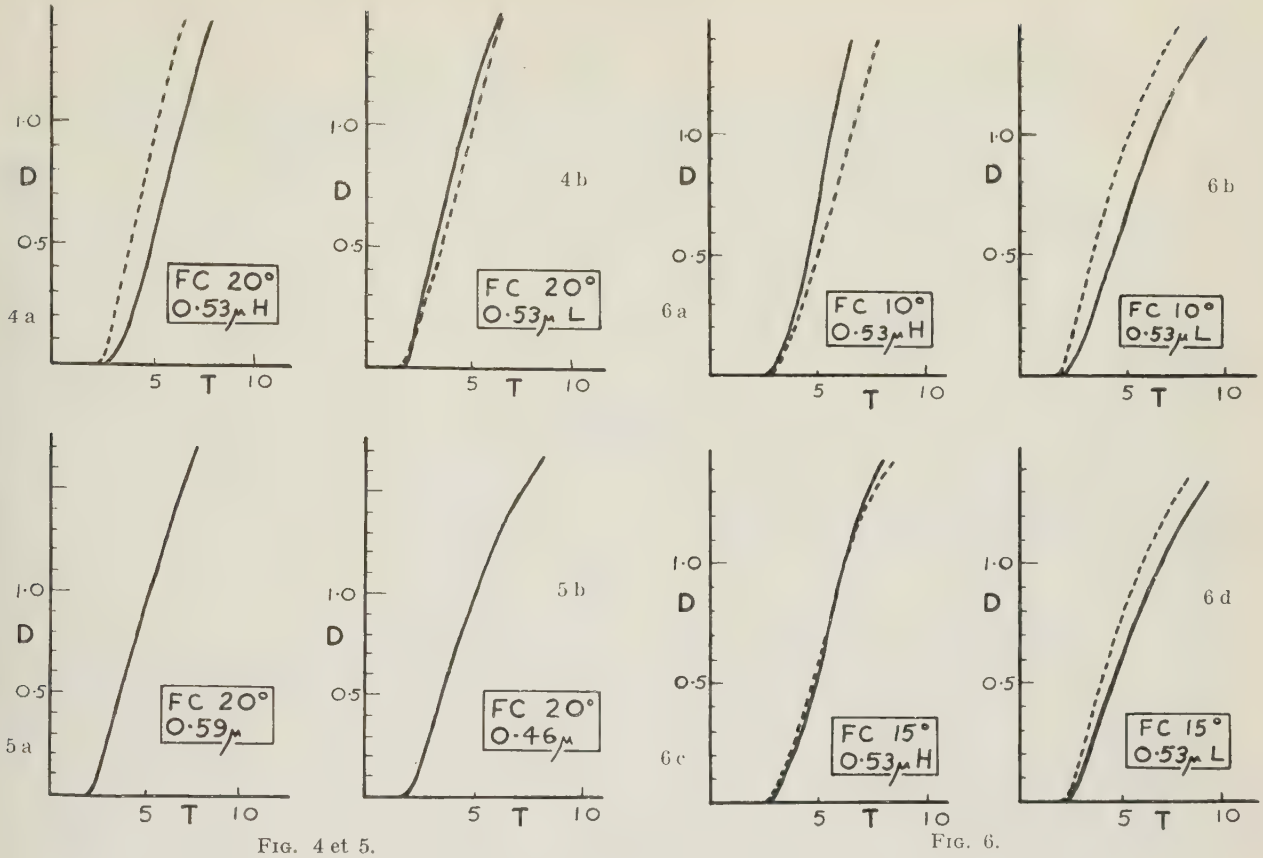


Fig. 4 et 5. Fig. 6.

It should be noted that, as in all binocular matching, the observer cannot view both patches foveally at the same time ; fixation had to be transferred from one to the other periodically. A fixation target was provided in the centres of both the test and the comparison fields, the subject fixating on the test for about 2 seconds, glancing across to the comparison and back, and refixating the test patch for a further two seconds, and so on. Thus the foveal recording were not made under the same conditions as those in the extra-fovea, hence the results which appear in figure 9 should be accepted with caution.

The curves shown in figure 2 to 14 give the differential local adaptation of the specified retinal location with respect to the adaptation of the foveal comparison area ; if there were no change of sensitivity of the macula, then these curves would give the amount and the rate of extrafoveal adaptation directly. It was anticipated that, with an initially light adapted fovea, the effect of reducing the comparison patch intensity by a factor of 1.5 log. units would itself cause only a small adaptation, i. e. the change of sensitivity. Nevertheless, in order to measure this change of sensitivity another binocular experiment was devised. Considering the results for the paracentral region, figures 2, 3, it will be seen that after the latent period, the comparison patch is reduced in luminance by up to about 1.4 log. units in 4 seconds : in order to simulate this the experimenter introduced a 1.4 density filter

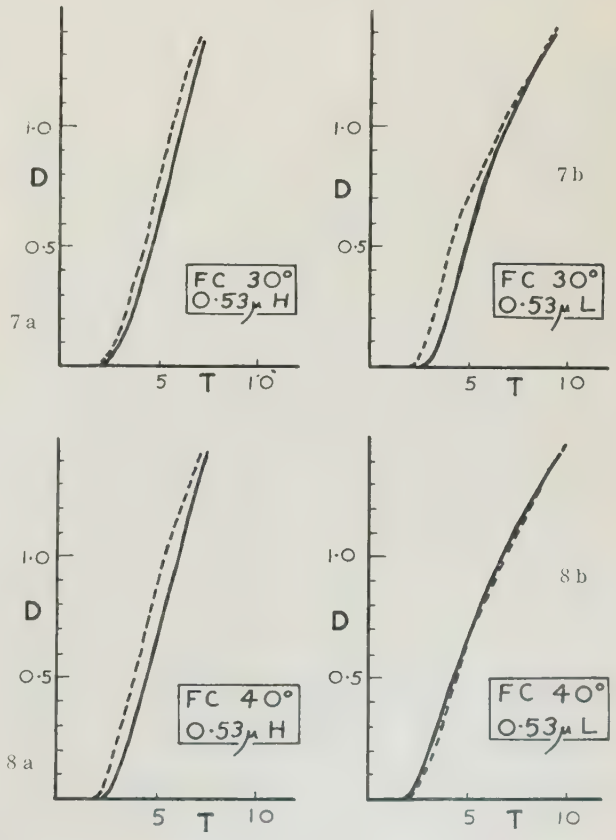


Fig. 7 et 8.

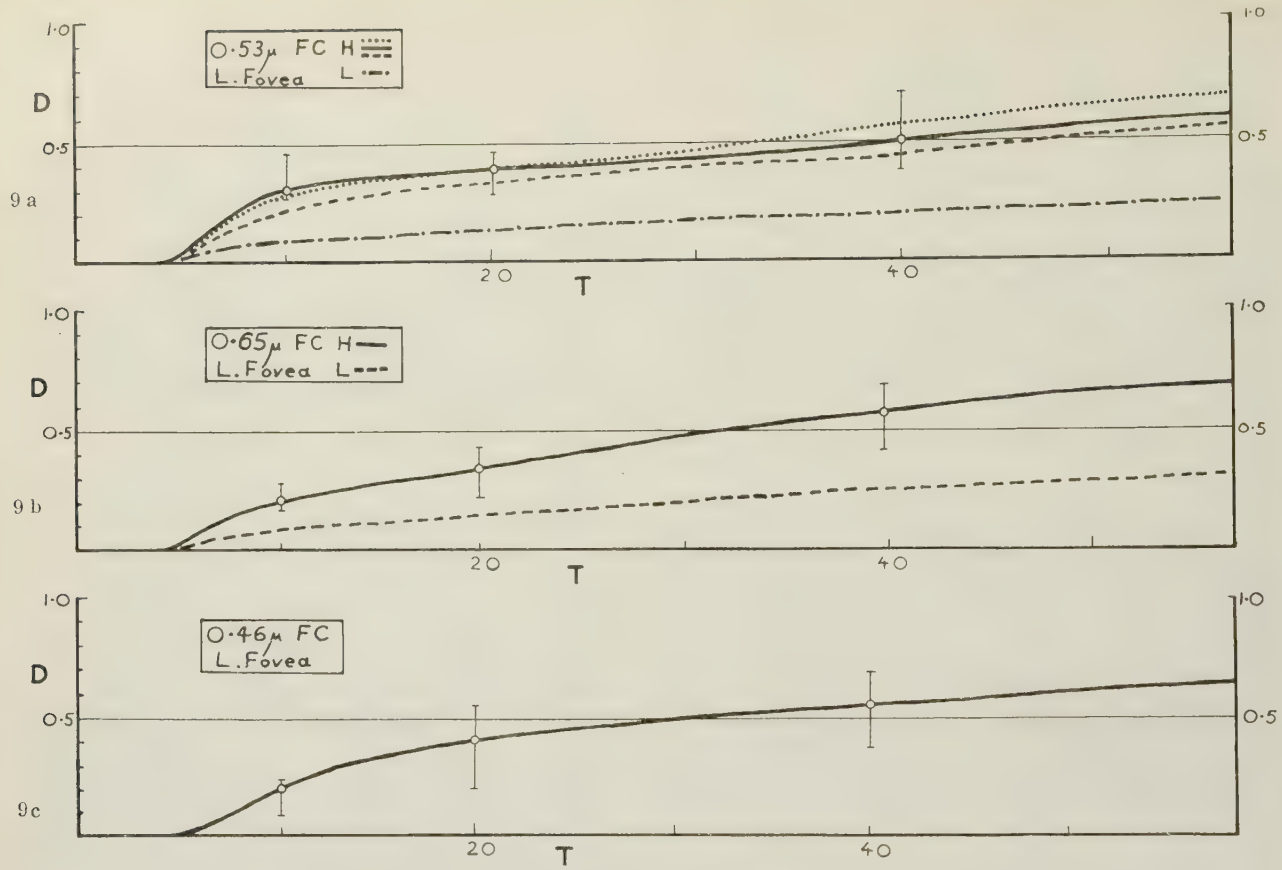


Fig. 9. — Course of foveal light adaptation; spread indicators at $T = 10$, 20, and 40 secs.

into a test beam, the reduction of luminance being discontinuous.

The experimental procedure was (1) binocular dark adaptation, (2) binocular foveal light adaptation, the left fovea viewing a test patch of the same luminance as the initial comparison patch in the main experiments, the right fovea viewing a patch of lower luminance such that when (3) a 1.4 filter was inserted in the left beam at $T = 0$ second, an initial match of brightness was obtained ; subsequently the wedge in the right beam (comparison) was moved by the crank with reduction of density to maintain equality of brightness. It was found that there was a very slow change of sensitivity for initial test stimuli of 0.65 μ, 0.53 μ *H*, 0. 53 μ *L*, and 0.46 μ (as for the initial levels for the comparison patch in the main experiments). In no case did a just noticeable difference (binocular matching) occur before about 20 seconds had elapsed. Thus the adaptation data of figures 2 to 9 need no significant correction for foveal changes of sensitivity, so giving directly the course of extra-foveal fading.

**Summary of results.** — The most important aspects of the observations are given below :

(1) There is always a delay time or latent period $T_d$ seconds.

(2) For a given observer, ceteris paribus :

(*a*) $T_d$ varies slowly and continuously with θ,

(*b*) $T_d$ decreases with increase of θ (see figure 15),

(*c*) $T_d$ does not depend on intensity,

(*d*) $T_d$ does not depend on wavelength.

(3) Different observers show significant individual differences in $T_d$.

(4) $T_d$ is usually in the range of 1 to 10 seconds.

(5) After the delay period there is always a period of rapid adaptation.

(6) The maximum rate of fading tends to increase with θ.

(7) The total extent of rapid fading increases with initial brightness for θ less than 8°.

(8) The total extent of rapid fading increases with θ, up to about 8° for most observers.

(9) For larger eccentricities, all observers state that the patch " vanishes " after rapid fading.

(10) Surrounding the patch is perceived a large diffuse cloud or halo, most noticeable at about 15 deg. and minimal for small θ.

(11) The cloud fades slowly, but only vanishes completely for large θ (above 30°).

(12) After the fast adaptation of the patch, there is a slow phase of the adaptation, for θ less than about 8 deg. (figs. 2, 3, 10 *a*, 11, 13 *a*).

In figures 15, 16 are collected certain retinal data for F. C., figure 15 showing the delay time $T_d$ as a

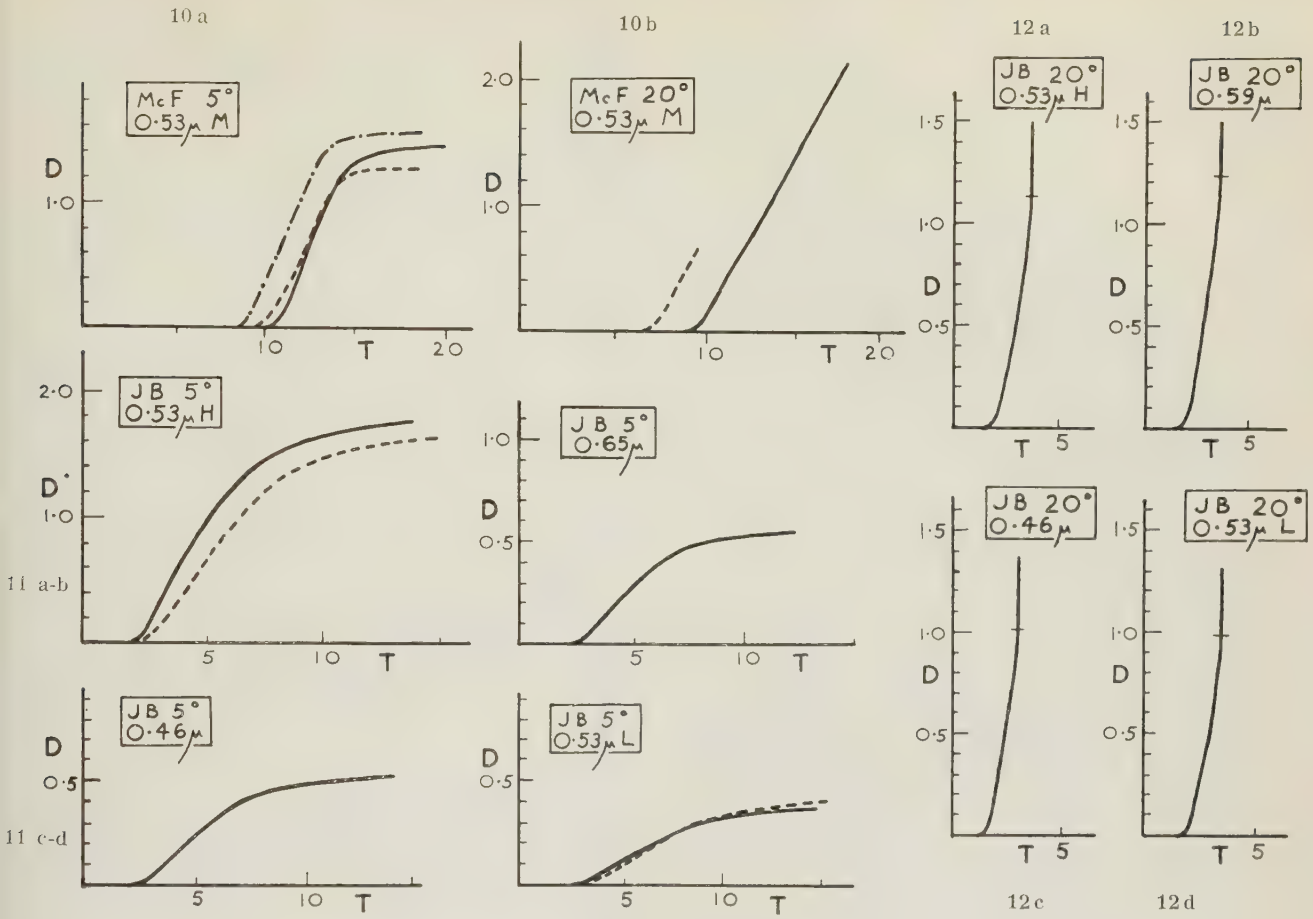


Fig. 10, 11, 12.

function of eccentricity for the brightness levels of 0.53 μ *H* and 0.53 μ *L*, while figure 16 gives the sensitivity data across the dark adapted retina in terms of the initial intensity $I_0$ required to match the constant foveal levels 0.53 μ *H* and *L*.

In connection with point (4) above it should be noted that one observer was found whose delay period $T_d$ was rather large (20 seconds). It is interesting to note that no after-images were observed, except by the anomalous observer D. P.

**Discussion.** — The diffuse cloud round the patch mentioned in sections (10) and (11) is probably due to scattering of light in the ocular media, possibly with a contribution from the effect of lateral interaction in the retina.

The sensitivity data of figure 16 suggest that at the brightness levels *L* and *H*, the visual response is typical of neither the scotopic nor photopic states (cf. Stiles and Crawford [14] and Rönne [15], Weale [16] respectively) ; it is to be noted that no reliable data are yet available for the sensitivity across the photopic retina. However it is clear that for the low level *L* the visual response is rod-dominated, while for the high level *H* the response has comparable contributions from the rods and cones.

The fact that $T_d$ is independent of wavelength or intensity but varies slowly with eccentricity indicates that the same mechanism is responsible for the fading process with all stimulation conditions of a dark adapted retina, the exact kinetics depending on the anatomical structure of the location concerned. The retina shows a continuous variation in properties from the rod-free central fovea, with its absence of neural convergence or horizontal connections and with little interaction, summation or occlusion, to the periphery, with maximum manifestation of these characteristics and maximum rod-to-cone density ratio. All this, together with the point (5) above which seems to hold even at the fovea where the rapid adaptation is only residual, shows that the mechanism responsible is characteristic of both rod and cone units.

The point (7) above leads to two possible interpretations : (*a*) rods show the rapid fading more markedly than cones, the increase in adaptation with the increase of θ being merely a consequence of the increasing rod-to-cone density ratio, or (*b*) the amount of rapid fading is determined ceteris paribus by the type of neural pathway between the primary receptors and the cortical projection, the increase with θ being a consequence of the increasing neural convergence and horizontal ramifications in the peripheral retina.

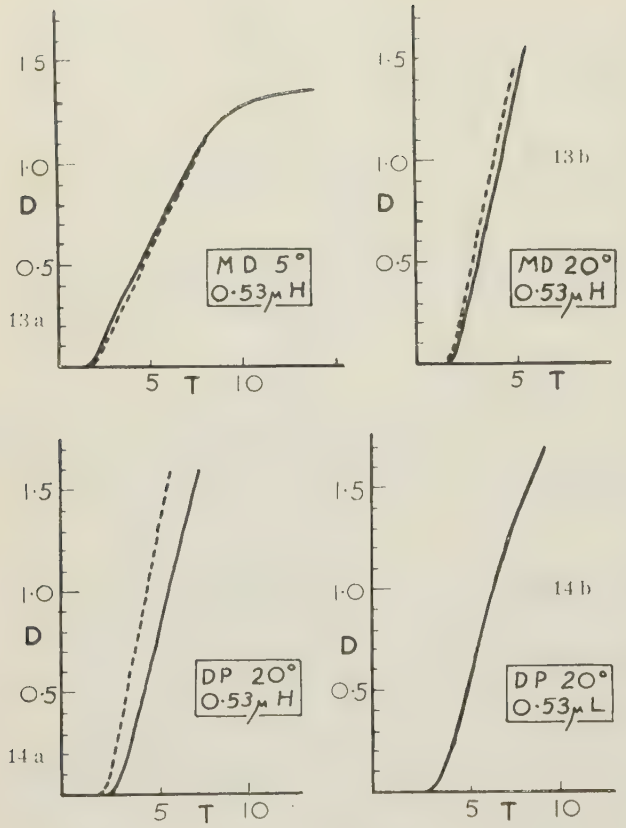


Fig. 13 and 14.

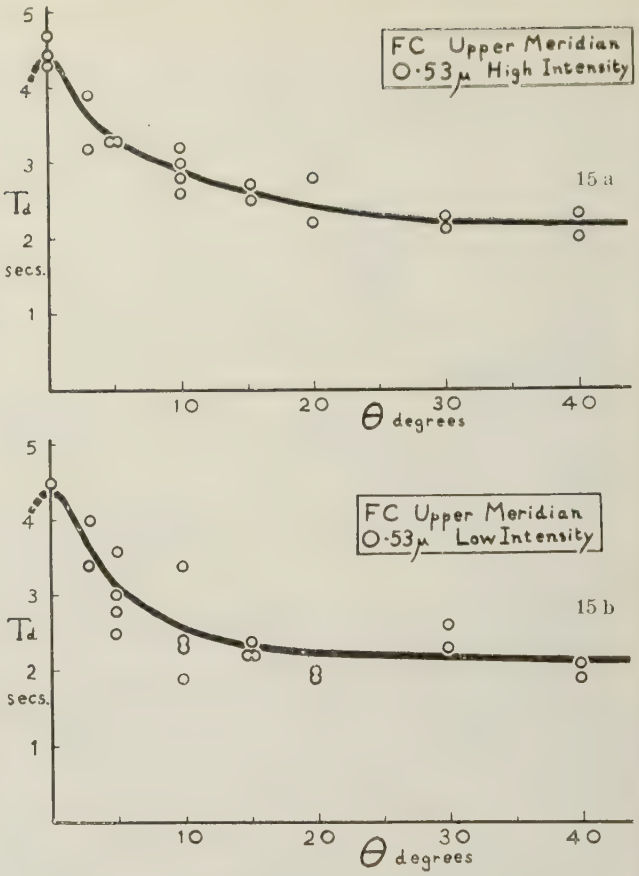


Fig. 15. — Delay time $T_d$ as a function of eccentricity.

Classical work [12, 13], on foveal light adaptation has established the very fast α-adaptation, complete within 1/10 second and the slow β-adaptation, complete to within 10 % of the ultimate level in 100 seconds. For the data presented the α-adaptation occurs too rapidly to be perceived in such a matching process, merely resulting in a change of absolute level, and not affecting the results. However the data establish a third component of adaptation, intermediate in rate between α-and β-adaptation, complete in a few seconds and inhibited by eye-movements. It is natural to identify the slow adaptation, which follows the local adaptation effect in the para-central region [ point (12) above ], with the β-adaptation process. In the past the tendency has been to assume the α-adaptation to be some form of electrical inhibition and the β-adaptation to be related to a photo-chemical bleaching ; if this be so, then the origin of the local adaptation effect needs an explanation. It is probable, however, that these views of α-and β-adaptation are but crude approximations to reality.

The possibility that the subjective fading process is due to a suppression in the cortex may be eliminated by the following consideration : for para-central stimulation a small shift of fixation of a few minutes of arc, after the fast fading has occurred, causes a bright fringe to appear where fresh retina is stimulat-

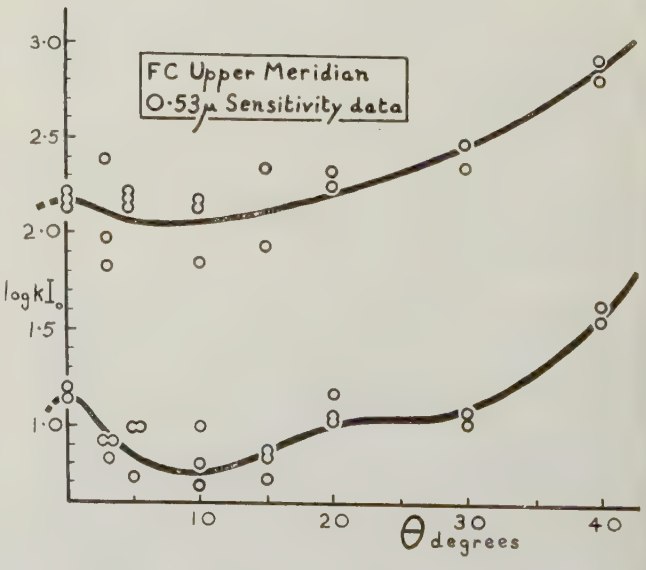


Fig. 16. — Luminance required to achieve constant initial subjective brightness across the retina. Upper curve --- level $H$ ; lower curve --- level $L$. The values from the left fovea are normalised so as to eliminate the effect of difference in sensitivity for the two eyes. Zero point of luminance scale represents 1.5 cd./sq. m.

ed, figure 1c, It is inconceivable that suppression could be so selective as to be restricted to areas no less sharply defined than corresponds to extra-foveal acuity.

In conclusion the similarity should be noted between the extra-foveal fading under voluntary fixation reported here and the loss of acuity and fading of foveal objects on a dark ground found with stabilised retinal images by DITCHBURN and co-workers [17-19]. It is possible that results reported here represent merely a particular case of the stabilised image effect, and that the very imperfect " stabilisation " is sufficient for a peripheral test patch because of the poor acuity there ; this hypothesis does not explain the relatively small changes in $T_d$ with eccentricity, figure 15, or the fact that fast fading appears to be residually present even in the central fovea, where a high perfection of stabilisation is necessary for a rapid decay of acuity. It is interesting to note that it has been found [19] that the total fading time at the fovea for a stabilised image is constant at three and six seconds for two observers in the intensity range given by 100 to 530 trolands ; this is comparable with the results quoted here, the range of brightness covered by 0.53 $\mu$ light being given by $9.3.10^1$ to $7.9.10^3$ foveal trolands.

**Acknowledgments**. — The project was commenced by Mlle M. JEANNE, who was with us for three months on a *British Council Scholarship*, and by J. D. MORELAND. The author is indebted to his colleagues who acted as observers, and to Prof. W. D. WRIGHT for his constant guidance and for suggesting the problem. Thanks are due to the *Medical Research Council* for their financial support.

REFERENCES

1. R. A. WEALE, *J. Physiol.*, **113**, 1951, 115.
2. R. A. WEALE, *Ibid.*, **114**, 1951, 435.
3. R. A. WEALE, *Ibid.*, **119**, 1953, 170.
4. J. D. MORELAND, *Opt. Acta*, **2**, 1955, 101.
5. J. D. MORELAND, Ph. D. Thesis, London, 1955.
6. D. TROXLER, *Ophthalm. Bibliothek*, Himly u. Schmidt, Jena, (1) s. l., 1804.
7. S. HOLTH, *Norsk Mag. for Laegevidenskaben, Kristiania*, 1896.
8. K. DUNLAP, *Amer. J. Physiol.*, **55**, 1920, 201.
9. R. GRANIT & W. VON AMMON, *Amer. J. Physiol.*, **95**, 1930, 229.
10. P. REEVES, *J. O. S. A.*, **4**, 1920, 35.
11. W. D. WRIGHT, « *Researches on Normal and Defective Colour Vision* ». Kimpton, London, 1946.
12. W. D. WRIGHT, *Proc. Roy. Soc.*, **115 B**, 1934, 49.
13. J. F. SCHOUTEN & L. S. ORNSTEIN, *J. O. S. A.*, **29**, 1939, 168.
14. W. S. STILES & B. H. CRAWFORD, *Proc. Roy. Soc.*, **122 B**, 1937, 255.
15. H. RÖNNE, *Arch. f. Augenheilk*, **78**, 1915, 284.
16. R. A. WEALE, *Brit. J. Ophthalm.*, **40**, 1956, 392.
17. R. W. DITCHBURN & D. H. FENDER, *Opt. Acta*, **2**, 1955, 128.
18. R. W. DITCHBURN & R. M. PRITCHARD, *Nature*, **177**, 1956, 424.
19. D. H. FENDER & R. M. PRITCHARD, (private communication), 1956.

*Manuscrit reçu le 19 novembre 1956*

**Lettre à l'éditeur**

## Zur Berechnung von Wellenflächen

JOHANNES PICHT
Potsdam-Griebnitzsee

In einer in Band 3 dieser Zeitschrift erschienenen Arbeit [1] gleichen Titels beschäftigt sich Herr F. I. HAVLIČEK mit einem Teilergebnis meiner gleichfalls in Band 3 dieser Zeitschrift erschienenen Arbeit [2] « *Zur Frage der optischen Lichtweg-Längen zweier Strahlen zwischen Objektpunkt und bildseitigem Schnittpunkt beider Strahlen* ».

In dieser Arbeit hatte ich zur Berechnung des Lichtwegunterschiedes zweier vom gleichen Objektpunkt ausgehender Strahlen in ihrem bildseitigen Schnittpunkt zunächst für ein Strahlenbündel mit der sphärischen Aberration.

$$\Delta s' = a \operatorname{tg}^2 u' + b \operatorname{tg}^4 u' + c \operatorname{tg}^6 u' + d \operatorname{tg}^8 u' + \dots$$

die Gleichungen für die Koordinaten $\xi$, $\rho$ der zugehörigen Wellenflächenschar angegeben, u. zw. gleichfalls als Potenzreihen von tg $u'$. Für die zugehörigen Koeffizienten ($a'$, $b'$, $c'$, $d'$, ...), die sich natürlich aus den Koeffizienten $a$, $b$, $c$, ... von $\Delta s'$ ergeben, wurden von mir die streng gültigen Formeln

$$a' = a - \frac{4}{3} b' ; b' = b - \frac{6}{5} c' ; c' = c - \frac{8}{7} d' ;$$

$$d' = d - \frac{10}{9} e' ; \dots$$

angegeben (1).

Herr HAVLIČEK wendet dagegen ein, dass es für eine strenge Darstellung vorzuziehen sei, bei der Rekursion « von niedrigerer zu höherer Ordnung » fortzuschreiten. Insbesondere scheint ihm zu missfal-

(1) Die von Herrn HAVLIČEK benutzten Koeffizienten $A$, $B$, $C$, ... der nach Potenzen von $u'$ (nicht : tg $u'$) entwickelten Wellenflächenkoordinaten weichen von meinen $a'$, $b'$, $c'$, ... naturgemäss ab, besitzen aber trotzdem eine weitgehende Ähnlichkeit, wenn man beachtet, dass die $A$, $B$, $C$, ... von Herrn HAVLIČEK meinen $a'$, $\frac{1}{3} b'$, $\frac{1}{5} c'$, ... entsprechen.

len, dass man — um zu besseren Näherungen zu kommen und zu grösseren Entfernungen von der Achse fortzuschreiten, wenn man also *nachträglich* noch höhere Potenzen von tg $u$ berücksichtigen will — die auf den rechten Seiten der Gleichungen von $a'$, $b'$, $c'$, $d'$, ... auftretenden $b'$, $c'$, $d'$, $e'$, ... ändern muss, also zu den bereits berechneten $a'$, $b'$, $c'$, $d'$, ... nicht nur einfach ein Korrektionsglied hinzuzufügen braucht.

Dieser Einwand des Herrn HAVLIČEK ist aber nicht zutreffend. Denn die von mir angegebenen Ausdrücke lauten ja — ausführlicher geschrieben — :

$$a' = a - \frac{4}{3} b + \frac{4.6}{3.5} c - \frac{4.6.8}{3.5.7} d + \frac{4.6.8.10}{3.5.7.9} e - \ldots +$$

$$b' = b - \frac{6}{5} c + \frac{6.8}{5.7} d - \frac{6.8.10}{5.7.9} e + \frac{6.8.10.12}{5.7.9.11} f - \ldots +$$

$$= \frac{3}{4} (a - a')$$

$$c' = c - \frac{8}{7} d + \frac{8.10}{7.9} e - \frac{8.10.12}{7.9.11} f + \frac{8.10.12.14}{7.9.11.13} g - \ldots +$$

$$= \frac{5}{6} (b - b')$$

$$d' = \frac{7}{8} (c - c').$$

$$e' = \frac{9}{10} (d - d')$$

.
.
.

Sie lassen sich also in einfachster Weise — bei Hinzunahme weiterer Glieder der Reihenentwicklung von $\Delta s'$ nach Potenzen von tg $u'$ — sofort ergänzen bzw. zahlenmässig verbessern. Das Entsprechende gilt auch für die von mir in der angegebenen Arbeit gleichfalls mitgeteilten Formeln für die Berechnung der Meridiankurve eines komabehafteten Strahlenbündels. Die dort von mir durch $B_2$, $B_4$, $B_6$, $B_8$, ... und $B_1$, $B_3$, $B_5$, $B_7$, ... bezeichneten Koeffizienten der $\xi$, $\eta$-Koordinaten der betreffenden Meridiankurve der Wellenflächenschar lauten — ausführlich geschrieben —

$$B_1 = a_1 - \frac{3}{2} a_3 + \frac{3.5}{2.4} a_5 - \frac{3.5.7}{2.4.6} a_7 + \frac{3.5.7.9}{2.4.6.8} a_9 - \ldots +$$

$$B_3 = a_3 - \frac{5}{4} a_5 + \frac{5.7}{4.6} a_7 - \frac{5.7.9}{4.6.8} a_9 + \\ + \frac{5.7.9.11}{4.6.8.10} a_{11} - \ldots +$$

$$= \frac{2}{3} (a_1 - B_1)$$

$$B_5 = a_5 - \frac{7}{6} a_7 + \frac{7.9}{6.8} a_9 - \frac{7.9.11}{6.8.10} a_{11} + \\ + \frac{7.9.11.13}{6.8.10.12} a_{13} - \ldots +$$

$$= \frac{4}{5} (a_3 - B_3)$$

$$B_7 = \frac{7}{6} (a_5 - B_5)$$

$$B_9 = \frac{8}{9} (a_7 - B_7)$$

.
.
.

sowie

$$B_2 = a_2 - \frac{4}{3} a_4 + \frac{4.6}{3.5} a_6 - \frac{4.6.8}{3.5.7} a_8 + \\ + \frac{4.6.8.10}{3.5.7.11} a_{10} - \ldots +$$

$$B_4 = a_4 - \frac{6}{5} a_6 + \frac{6.8}{5.7} a_8 - \frac{6.8.10}{5.7.9} a_{10} + \\ + \frac{6.8.10.12}{5.7.9.11} a_{12} - \ldots +$$

$$= \frac{3}{4} (a_2 - B_2)$$

$$B_6 = a_6 - \frac{8}{7} a_8 + \frac{8.10}{7.9} a_{10} - \frac{8.10.12}{7.9.11} a_{12} + \\ + \frac{8.10.12.14}{7.9.11.13} a_{14} - \ldots +$$

$$= \frac{5}{6} (a_4 - B_4)$$

$$B_8 = a_8 - \frac{10}{9} a_{10} + \frac{10.12}{9.11} a_{12} - \frac{10.12.14}{9.11.13} a_{14} + \\ + \frac{10.12.14.16}{9.11.13.15} a_{16} - \ldots +$$

$$= \frac{7}{8} (a_6 - B_6)$$

$$B_{10} = a_{10} - \frac{12}{11} a_{12} + \frac{12.14}{11.13} a_{14} - \frac{12.14.16}{11.13.15} a_{16} + \\ + \frac{12.14.16.18}{11.13.15.17} a_{18} - \ldots +$$

$$= \frac{9}{10} (a_8 - B_8)$$

.
.
.

Es bietet also — wie oben schon erwähnt — keinerlei Schwierigkeit, bei Hinzunahme weiterer Potenzen von tg $u'$ bzw. tg $k'$ die dadurch bedingten Änderungen bzw. Korrektionsglieder der $a'$, $b'$, $c'$, ... bzw. der $B_\nu$ an diese anzubringen.

*Manuscrit reçu le 20 janvier 1957.*

[1] F. I. HAVLIČEK, *Opt. Acta* **3**, 147, 1956.
[2] J. PICHT, *Opt. Acta*, **3**, 1, 1956.

## Bibliographie

Johannes Picht. **Vorlesungen über Atomphysik,** Band 1. VEB Deutscher Verlag der Wissenschaften Berlin 1956, 238 Seiten.

Es erscheint ungemein schwierig, eine Theorie der Atomphysik zu versuchen, ohne durch die ausführliche Behandlung der theoretischen Mechanik, Wärmelehre und Elektrizität auf diese Aufgabe hinreichend vorzubereiten. Es überrascht deswegen, wie es dem Verfasser gelungen ist, die aus diesen Gebieten notwendigen Grundlagen in einer so knappen un doch verständlichen Form zu schaffen. So sind die allgemeinen Prinzipien, der Mechanik in die Statistik eingeschaltet worden und erlauben dann die Behandlung der Statistik unter Benutzung der generalisierten Koordinaten. Die Darlegung der Theorie des Wärmestrahlung führt anschliessend von der Statistik zur Quantenvorstellung, auf die sich die Behandlung des Baues und der Strahlung der Atome und Moleküle aufbaut. Mit der Einführung des Pauli-Prinzips wird aber der klassischen Statistik eine der wichtigsten Voraussetzungen entzogen. Deswegen schliesst der 1. Band mit der neueren Fassung der Statistik im Sinne von Bose-Einstein und Fermi-Dirac. Der noch nicht erschienene 2. Band soll die Wellenmechanik und Kernphysik bringen. Das Buch ist aus den Vorlesungen des Verfassers erwachsen und trägt damit die Kennzeichen eines gut verständlichen Leitfadens, der den Studenten durch das Gebiet der Atomphysik führt.

J. Picht, **Zur Theorie der Totalreflexion**. Abhandlungen der Deutschen Akademie der Wissenschaften zu Berlin. Klasse für Mathematik, Physik und Technik, 1955 Nr. 2. Brosch. DM 9,

Der Verfasser hat seit 1925 in mehreren Arbeiten das Problem der Reflexion und Brechung von Lichtwellen an der ebenen Trennungsfläche zweier optischer Medien beugungstheoretisch behandelt, und zwar ausgehend von einer von ihm angegebenen Integraldarstellung beliebig deformierter Wellenflächen. (Man vergleiche hierzu etwa J. Picht, Optische Abbildung, Vieweg & Sohn, Braunschweig 1931).

In der vorliegenden Abhandlung gibt der Verfasser eine Zusammenfassung seiner Untersuchungsergebnisse, die inzwischen z. T. experimentell bestätigt werden konnten. Das eigentümliche Verhalten des Poyntingschen Vektors an der Grenzfläche mit dem Übertritt von Energie in das dünnere Medium und ihrer Rückkehr in das dichtere Medium an anderer Stelle hat strahlenoptische Konsequenzen, die näher diskutiert werden : Es überlagert sich der « ideal », reflektierten Welle zusätzlich eine deformierte Welle, deren Strahlenbündel (Normalen der Wellenflächen) sphärischen Fehler bzw. Astigmatismus besitzen, je nachdem wie der erzeugende Dipol bzw. der Hertzsche Vektor gerichtet ist. Ausserdem können Strahlversetzungen senkrecht zur Einfallsebene auftreten, so dass man einem einfallenden Strahl nicht mehr ohne weiteres als Fortsetzung einen reflektierten Strahl zuordnen kann. Jedenfalls liegt er im allgemeinen nicht mehr in der Einfallsebene.

Velte.

Glenn A. Fry, **Blur of the retinal image**. The Ohio State University Press, Columbus. 1955. pp. xxxiii + 120.

Professor Fry's monograph is not specifically addressed, but it appears to be directed to the advanced student of ophthalmological optics who, while not mainly interested in mathematical theory, needs a straightforward mathematical treatment of the factors operating to produce blur in the retinal image. Questions of two kinds are discussed. An examination is made of the distribution of light on the retina when the object is a monochromatic point source and the degradation of the ideal punctiform image occurs through incorrect focus or astigmatism (approximation of geometrical optics), or through diffraction, with and without incorrect focus and spherical aberration. The second question is the summation of point source distributions to give the resultant distributions for polychromatic point sources, for line objects of different widths and for a linear boundary separating extended light and dark areas. The last case provides the basis for an " index of blur " defined as the reciprocal of the space gradient of illumination across the boundary, taken at the line of the geometric image. Once the degradation of the point source image is known this index is calculable. The author attaches much importance to the index and although it is not a very deep concept its convenience for comparing the effects on blur of the various factors is established.

Since the appearance of this book the Ivanoff values for the spherical aberration of the eye have been amended, so that the effects of such aberration on blur as calculated by the author would be even smaller than he found. It is also a pity that the objective measurements of light distribution in retinal images by M^lle^ Flamant appeared too late for inclusion.

Professor Fry has obviously been at pains to see that the reader follows every detail of his calculations — twenty introductory pages are devoted to explanations of symbols — and the derivation of the formulae tends to over-balance the discussion of their implications. But for the class of student mentioned this should prove a most useful text. Professor Fry makes tantalising references to further developments in the subject, which we may hope to have expounded by him with equal clarity in a subsequent monograph.

W. S. S.

**Astronomical Optics and related Subjects.** Publié sous la direction du Prof. Zdenek Kopal (Université de Manchester) North-Holland Publishing Company, Amsterdam, 1956.

Cet ouvrage rassemble la plupart des communications présentées au colloque tenu à Manchester du 19 au 22 avril 1955. Le but de ce colloque était d'assurer un contact entre les astronomes et les opticiens, de confronter les progrès effectués et d'attirer l'attention des chercheurs opticiens sur les problèmes astronomiques. On trouve dans l'ouvrage un ensemble d'exposés très intéressants sur les questions théoriques ou instrumentales à l'ordre du jour.

La table des matières est ainsi constituée :

I. *Information theory and optics.* — D. Gabor : Light and information. A. Blanc-Lapierre, M. Picibono, and M. Savelli : Mesures sur le bruit de fond en optique. E. H. Linfoot : Noise, aberrations, and the information content of optical images. P. M. Duffieux : Aspects du problème de l'objet. D. Gabor : Collecting information on partially known objects.

II. *Optical images and diffraction.* — E. H. Linfoot : Transmission factors and the assessment of optical image quality. J. Kammerer : Ein Verfahren zur Raschen Ermittlung der Definitionshelligkeit. J. M. Naish : On the distribution of light within small optical images. P. M. Dumontet : La correspondance objet-image en optique. G. Lansraux : Filtre d'amplitude-diaphragme tournant. J. Picht : Investigations concerning geometrical and wave theoretical images formed by a paraboloidal mirror. F. D. Kahn : The basic approximations in the theory of phase-contrast microscope. A. Nisbet : Reduced hertzian potentials and their sources. R. C. Spencer : Antennas for radio astronomy. B. Roizen-Dossier : L'apodisation des images optiques ; cas particulier de l'obturation centrale.

III. *Interferometry and coherence problems.* — E. Wolf : The coherence properties of optical fields. H. Siedentopf : A remark on the interferometry of circular sources. L. R. Baker : An interferometer for measuring the response of an optical system to spatial frequencies. G. Courtes : Techniques d'observation de l'émission monochromatique interstellaire.

IV. *Electronic devices in astronomical optics.* — J. D. McGee : Photo-electronic aids in astronomy. P. Fellgett : Theoretical and practical explorations of the use of television techniques in Astronomy. W. L. Wilcock and J. E. Geake : The design and operation of a photoelectric spectro-photometer. H. J. J. Braddick and W. L. Wilcock : A multiplex photoelectric spectrophotometer. W. R. Bradford : A wide-range photoelectric photometer. G. Black : Electronic digital computers and optics. A. W. Hanson, C. A. Taylor and H. Lipson : The application of image-storage devices to the presentation of optical diffraction patterns.

V. *Resolution problems and scintillation.* — V. Ronchi : New ideas on optical images and resolving power. A. W. Hanson and C. A. Taylor : experimental study of resolving power. N. S. Kapany : A light funnel for stellar spectrograph. M. A. Ellison : The effects of scintillation on telescopic images. R. Fürth : Statistical analysis of scintillations of stars. J. Rösch : Etude de l'agitation des images télescopiques par la méthode de Hartmann. H. Siedentopf : Scintillation and photometric accuracy. T. Kaiser : A theory of stellar scintillation. P. Fellgett : On scintillation.

VI. *Wide-angle optical systems and aspheric surfaces.* — H. Slevogt : Das Problem der Eindeutigkeit bei der Bestimmung von Rotationssymmetrischen asphärischen Flächen. B. Richards. Diffraction in systems of high relative aperture. W. Weinstein and J. A. Dobrowolski : Production of aspheric surfaces by vacuum deposition. J. H. Bigay : Utilisation d'une surface asphérique dans un spectrographe à miroirs de grande ouverture relative. Ch. Fehrenbach : La mesure des vitesses radiales des étoiles au prisme objectif. A. C. S. van Heel : Determination of changes of optical axis of the telescope of a meridian circle.

VII. *Filter photography and thin films.* — J. Ring : The Fabry-Pérot interferometer in Astronomy. Z. Kopal and P. Y. Millns : Dye filters for wide-angle astronomical photography. O. S. Heavens and S. D. Smith : Multi-layer filters in the infrared. W. Weinstein : A new kind of interference filter. P. Giacomo : Préparation et performance des filtres interférentiels diélectriques dans le visible et l'infrarouge ; effets de la diffusion. J. Rösch : Concluding remarks.

N° d'éditeur 129. — *Revue d'optique.* — *Le Directeur :* Emile Perrin.
Commission paritaire des papiers de Presse n° 29754

3565. — Imprimerie JOUVE, 15, rue Racine, Paris. — 7-57